Non-Markovian barrier crossing with two-time-scale memory is dominated by the faster memory component

Julian Kappler, Victor B. Hinrichsen, and Roland R. Netz

Freie Universität Berlin

(Dated: July 31, 2019)

We investigate non-Markovian barrier-crossing kinetics of a massive particle in one dimension in the presence of a memory function that is the sum of two exponentials with different memory times τ_1 and τ_2. Our Langevin simulations for the special case where both exponentials contribute equally to the total friction show that the barrier crossing time becomes independent of the longer memory time if at least one of the two memory times is larger than the intrinsic diffusion time. When we associate memory effects with coupled degrees of freedom that are orthogonal to a one-dimensional reaction coordinate, this counterintuitive result shows that the faster orthogonal degrees of freedom dominate barrier-crossing kinetics in the non-Markovian limit and that the slower orthogonal degrees become negligible, quite contrary to the standard time-scale separation assumption and with important consequences for the proper setup of coarse-graining procedures in the non-Markovian case. By asymptotic matching and symmetry arguments, we construct a crossover formula for the barrier crossing time that is valid for general multi-exponential memory kernels. This formula can be used to estimate barrier-crossing times for general memory functions for high friction, i.e. in the overdamped regime, as well as for low friction, i.e. in the inertial regime. Typical examples where our results are important include protein folding in the high-friction limit and chemical reactions such as proton-transfer reactions in the low-friction limit.

I. INTRODUCTION

Rare events, such as chemical reactions, macromolecular conformational transitions, or nucleation events, can be modeled as barrier crossing in an effective one-dimensional energy landscape [1–5]. Due to the coupling to intra- and intermolecular orthogonal degrees of freedom, the dynamics of the reaction coordinate becomes non-Markovian and can be characterized by a memory function that describes for how long a system remembers its past state [6–11]. Memory effects have been studied in the context of ion-pair kinetics [12, 13], conformational transitions in small molecules [14–16], diffusive motion of particles and molecules in liquids [17–20], cell locomotion [21], polymer looping kinetics [22–26] and protein folding [27, 28], and have been demonstrated to substantially influence barrier-crossing times for slowly decaying memory functions [29–34].

In previous numerical studies concerned with position-independent memory effects on the barrier-crossing kinetics, the memory function has been assumed to be single exponential or single Gaussian and is thus chraracterized by a single time scale, the memory time τ_Γ [31, 33–36]. Even in this simple scenario the effect memory has on the time needed to cross the barrier, the mean-first passage time τ_{MFP}, is subtle: for a memory time τ_Γ that is longer than the intrinsic diffusion time scale and for fixed friction coefficient γ (defined by the integral over the memory function), τ_{MFP} scales as $\tau_{\mathrm{MFP}} \sim \tau_\Gamma^2 e^{\beta U_0}$, where U_0 denotes the barrier height and $\beta = 1/(k_B T)$ the inverse thermal energy [31, 36]. The exponential term corresponds to the Arrhenius law and is for many applications the dominant factor. In the present context we are mostly interested in the pre-exponential factor, which signals that the presence of memory modifies the

barrier-crossing kinetics even when the barrier-crossing time τ_{MFP} is much longer than the memory time τ_Γ; thus, a naive time-scale separation argument, according to which memory would only influence reaction kinetics up to times scales of the memory time itself, is not valid. For intermediate values of τ_Γ a distinct scaling regime exists, where memory in fact speeds up barrier-crossing kinetics, meaning that τ_{MFP} is significantly shorter than in the Markovian limit when τ_Γ tends to zero at fixed γ [36]. Thus, i) whether memory speeds up or slows down reaction kinetics depends on the precise value of the memory time, and ii) for long memory time τ_Γ the barrier-crossing time τ_{MFP} is influenced by memory effects even when $\tau_{\mathrm{MFP}} \gg \tau_\Gamma$.

While these results vividly demonstrate the complex influence of memory on reaction kinetics, they are of only limited practical use, since memory effects are typically caused by the reaction coordinate coupling to several orthogonal degrees of freedom and as a consequence memory functions are characterized by more than one time scale [12, 15, 18, 19, 37, 38]. Systematic numerical results on the effect of memory functions with more than one time scale on reaction kinetics have not been presented in literature.

In this work, we study the barrier-crossing dynamics of a massive particle in a one-dimensional double-well potential in the presence of a memory function that consists of the sum of two exponentials with different decay times τ_1 and τ_2. To limit the number of parameters in our simulations of the generalized Langevin equation (GLE), we consider the case where the two exponentials each contribute equally to the friction coefficient, i.e. when the integrals over each memory component are equal. Contrary to what one might intuitively expect, we find that in the asymmetric case $\tau_1 \ll \tau_2$, the barrier-crossing time

is solely determined by the memory contribution with the shorter memory time τ_1 if τ_2 exceeds the intrinsic diffusion time scale; this result is also predicted analytically by a pole analysis of the linearized Langevin equation. Our finding is at odds with standard time scale separation arguments and coarse graining procedures that are normally designed to project onto the slowest degrees of freedom [39–42]. We conclude that for non-Markovian barrier-crossing phenomena, in particular the coupling to the fast – not the slow – orthogonal degrees of freedom needs to be preserved in order to obtain an accurate description of the reaction kinetics.

Based on symmetry arguments and asymptotically valid rate expressions, we construct a heuristic crossover formula for the barrier-crossing time in a double well potential in the presence of a general multi-exponential memory kernel. This crossover formula not only accurately describes our numerical results for bi-exponential memory functions, it can also be used to estimate the effects general memory functions have on the reaction kinetics of experimental and simulation systems.

Our results are relevant for the description of the reaction kinetics of general non-Markovian systems. For example, pronounced memory effects are expected when the folding of a protein is described in terms of a reaction coordinate that does not properly describe all barriers relevant for the folding process [27]. The traditional approach would be to construct an improved reaction coordinate that shows minimal memory effects. We here consider an alternative modeling approach that includes non-Markovian effects, and in particular the fast-decaying memory contributions in order to correctly describe the reaction kinetics. One other example where strong memory effects are expected are fast chemical reactions in a solvent, for example proton-transfer reactions in water, where the motion along the reaction coordinate and solvent motion occur on the same time scale [43, 44]. Also here, a reduced description in terms of a low-dimensional reaction coordinate becomes valid if memory effects are properly included. Again, the quickly decaying memory contributions will be particularly important. Our paper is a first step towards the systematic usage of multi-scale memory functions for non-Markovian kinetic modeling.

II. MODEL FOR BARRIER CROSSING WITH TWO-TIME-SCALE MEMORY

We consider the one-dimensional generalized Langevin equation (GLE) [6, 7, 29, 33]

$$m\,\ddot{x}(t) = -\int_0^t \Gamma(t-t')\dot{x}(t')\,\mathrm{d}t' - U'(x(t)) + \eta(t), \quad (1)$$

where m is the effective mass of the reaction coordinate x, $\Gamma(t)$ is the memory function, $U'(x)$ denotes the derivative of the potential $U(x)$, and $\eta(t)$ is a time-dependent random force. The random force is Gaussian with zero
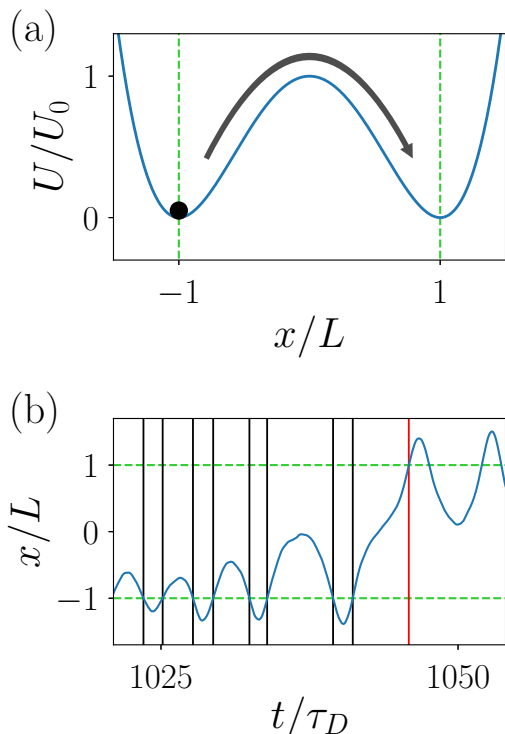

FIG. 1. (a) Illustration of the barrier crossing of a massive particle in the double-well potential $U(x)$ given by Eq. (2). The mean first-passage time τ_{MFP} is defined as the mean time difference between crossing the minimum at $x = -L$ (left dashed line) and crossing the other minimum at $x = L$ (right dashed line) for the first time. (b) Illustration of how first-passage times (FPTs) are obtained from Langevin simulations. Vertical black lines mark crossings of the trajectory with the potential minimum $x = -L$ (lower dashed horizontal line), the vertical red line marks the first crossing of the trajectory with the potential minimum $x = L$ (upper dashed horizontal line). Each vertical black line contributes to the ensemble of first-passage events and the corresponding FPT is obtained by calculating the time difference between the black and the red lines. The MFPT τ_{MFP} is obtained by averaging over all FPTs. For the simulation trajectory shown, the parameters $\tau_m/\tau_D = 10$, $\tau_1/\tau_D = \tau_2/\tau_D = 0.001$ and barrier height $\beta U_0 = 3$ are used.

mean, $\langle\eta(t)\rangle = 0$, and obeys the generalized fluctuation-dissipation theorem (FDT) $\beta\langle\eta(t)\eta(t')\rangle = \Gamma(|t-t'|)$. We consider a symmetric double-well potential

$$U(x) = U_0\left[\left(\frac{x}{L}\right)^2 - 1\right]^2, \quad (2)$$

illustrated in Fig. 1 (a), which is characterized by the barrier height U_0 and by the spatial separation $2L$ between the two potential wells. In our simulations we assume a bi-exponential memory function

$$\Gamma(t) = \sum_{i=1}^{2} \frac{\gamma_i}{\tau_i} \exp\left(-|t|/\tau_i\right) \quad (3)$$

where τ_1, τ_2 are two memory time scales and the corresponding friction coefficients are γ_1, γ_2. We call $\gamma = \int_0^\infty dt\, \Gamma(t) = \gamma_1 + \gamma_2$ the total friction coefficient. In our simulations we consider the special case where each of the two exponentials contributes equally to the total friction coefficient, i.e. $\gamma_1 = \gamma_2 = \gamma/2$. To reduce the number of parameters, we introduce the time scales

$$\tau_m = \frac{m}{\gamma}, \qquad \tau_D = \beta L^2 \gamma, \qquad (4)$$

where the inertial time τ_m characterizes viscous dissipation of particle momentum, and τ_D is the intrinsic diffusion time which depends on the barrier separation L and the total friction coefficient γ. Memory effects are important if the memory time exceeds τ_D. With these definitions, the bi-exponential system with $\gamma_1 = \gamma_2 = \gamma/2$ is determined by the three dimensionless time scale ratios τ_m/τ_D, τ_1/τ_D, τ_2/τ_D and the dimensionless barrier height βU_0, see Appendix A for details. In our simulations we use a fixed barrier height of $\beta U_0 = 3$, except in Appendix G where we also present results for higher values of βU_0.

To simulate the GLE numerically, we explicitly couple the particle coordinate x to two auxiliary degrees of freedom with relaxation times τ_1 and τ_2, see Appendix B for details. Using a fourth-order Runge-Kutta integration scheme, we then simulate the composite system in the parameter range $\tau_m/\tau_D \in [10^{-3}, 10^3]$, $\tau_1/\tau_D, \tau_2/\tau_D \in [10^{-3}, 10^2]$. Initial particle positions are sampled from a Gaussian approximation of the probability distribution in the left well around $x = -L$, i.e., $\langle x(0) \rangle = -L$, $\beta\langle(x(0) + L)^2\rangle = 1/U''(-L) = L^2/(8U_0)$. Initial velocities are sampled from a Gaussian distribution with zero mean and variance $\beta\langle\dot{x}^2(0)\rangle = 1/m$, in accordance with the equipartition theorem. The initial values for the auxiliary degrees of freedom are sampled from their corresponding equilibrium distributions, see Appendix B for details.

From our simulations we obtain distributions for the first-passage time (FPT) τ_{FP} defined by the time difference between crossing the potential minimum at $x = -L$ and reaching the potential minimum at $x = L$ for the first time, see Fig. 1 (b) for an illustration. Since the potential is symmetric, we also collect first-passage events from crossing $x = L$ and reaching $x = -L$ for the first time. The mean first-passage time (MFPT) τ_{MFP} is subsequently calculated by averaging over all individual first-passage events.

III. TRAJECTORIES AND FIRST-PASSAGE DISTRIBUTIONS

In Fig. 2 we show typical simulation trajectories that illustrate how the character of barrier-crossing events changes with varying mass, friction, and memory time parameters. In Fig. 2 (a), (b), (d), (e) the two memory times are equal, $\tau_\Gamma \equiv \tau_1 = \tau_2$, so that the memory

function is in fact single-exponential. For high friction and short memory in Fig. 2 (a), i.e. for $\tau_m/\tau_D \ll 1$ and $\tau_\Gamma/\tau_D \ll 1$, the barrier crossing is diffusive, meaning that the particle fluctuates in a potential well for a long time until a single barrier-crossing event occurs with a transition path time that is much shorter than the mean first-passage time [45, 46]. In contrast, if the friction is low or if the memory time is long, i.e. for $\tau_m/\tau_D \gg 1$ or $\tau_\Gamma/\tau_D \gg 1$, the trajectories in Fig. 2 (b), (d), (e) are characterized by bursts of multiple barrier recrossings. In these cases the barrier-crossing dynamics is dominated by the diffusive exchange of energy between the particle and the thermal bath; once the particle has acquired enough energy to cross the barrier, it oscillates back and forth between the two wells until its energy falls below the barrier energy again [36, 47]. Figure 2 (c) shows a trajectory for high friction $\tau_m/\tau_D = 0.001 \ll 1$ and different memory times $\tau_1/\tau_D = 0.001 \ll \tau_2/\tau_D = 10$. The trajectory looks similar to the high-friction short-memory trajectory for $\tau_m/\tau_D = 0.001$ and $\tau_1/\tau_D = \tau_2/\tau_D = 0.001$ shown in Fig. 2 (a), and is markedly different from the trajectory for $\tau_m/\tau_D = 0.001$ and $\tau_1/\tau_D = \tau_2/\tau_D = 10$ displayed in Fig. 2 (b), which is characterized by extended periods of multiple recrossings. We conclude that a high-friction trajectory that is governed by the sum of a slowly decaying memory contribution with $\tau_2/\tau_D = 10$ and a quickly decaying memory contribution with $\tau_1/\tau_D = 0.001$ looks like a trajectory with only short-time memory, meaning that the long-time memory contribution appears to be negligible compared to the short-time memory contribution. Similarly, the trajectory for low friction $\tau_m/\tau_D = 10 \gg 1$ and different memory times $\tau_1/\tau_D = 0.001 \ll \tau_2/\tau_D = 10$ shown in Fig. 2 (f) resembles more the low-friction Markovian trajectory for $\tau_m/\tau_D = 10$ and $\tau_1/\tau_D = \tau_2/\tau_D = 0.001$ in Fig. 2 (d) than the low-friction long-memory trajectory for $\tau_m/\tau_D = 10$ and $\tau_1/\tau_D = \tau_2/\tau_D = 10$ in Fig. 2 (e). Again, we observe that the slowly decaying memory contribution has a negligible effect on a low-friction trajectory in the presence of a second memory contribution with a much shorter memory time.

The analysis of first-passage-time (FPT) distributions allows a more quantitative comparison of barrier-crossing statistics. Fig. 3 presents numerically obtained FPT distributions in a semi-logarithmic representation, calculated for the same parameters as for the trajectories depicted in Fig. 2. For all parameter combinations considered, the distributions are well described by a single-exponential distribution

$$\rho(\tau_{\text{FP}}) = \frac{1}{\tau_{\text{MFP}}} \exp(-\tau_{\text{FP}}/\tau_{\text{MFP}}), \qquad (5)$$

shown as solid lines in Fig. 3. Only for the long-memory cases shown in Fig. 3 (b), (e) we see slight deviations from an exponential distribution for small τ_{FP}/τ_D, which we attribute to the presence of multiple recrossing events seen in the trajectories shown in Fig. 2 (b), (e), but which do not affect the MFPT significantly, as was previously
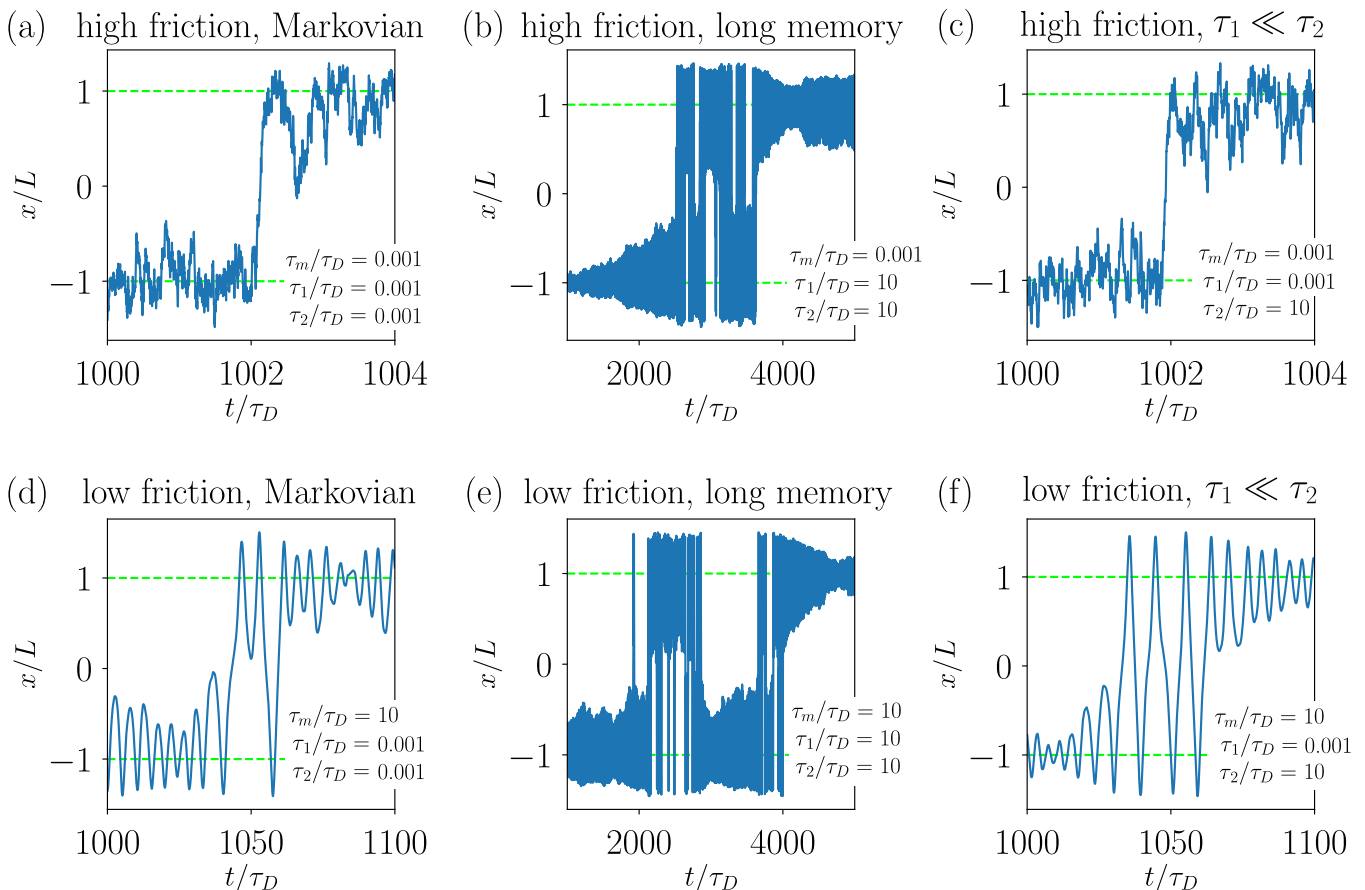
FIG. 2. Typical simulation trajectories that display barrier-crossing events for fixed barrier height $\beta U_0 = 3$. Simulation parameters used are given in the legends. The horizontal dashed lines indicate the minima of the quartic potential Eq. (2), which is shown in Fig. 1 (a).

demonstrated in Ref. [36]. Both for high friction (upper row) and low friction (lower row), we see that if the two memory times are very different, as in Fig. 3 (c), (f), the resulting FPT distribution is still single-exponential. Moreover, the MFPTs in Fig. 3 (c), (f) are close to the corresponding MFPTs for single-exponential memory with the shorter memory time, shown in Fig. 3 (a), (d), and differ by orders of magnitude from the single-exponential MFPTs for the longer memory time, shown in Fig. 3 (b), (e). We conclude that the barrier-crossing statistics in the presence of bi-exponential memory is characterized by single-exponential FPT distributions which are dominated by the shorter memory time. This result is corroborated by a pole analysis of the positional autocorrelation function obtained form the linearized generalized Langevin equation, see Appendix C, where we show that indeed for $\tau_D \ll \tau_1 \ll \tau_2$, the particle motion is dominated by τ_1.

IV. MFPT RESULTS FOR SINGLE-EXPONENTIAL MEMORY AND GENERAL CROSSOVER FORMULA

We first consider the symmetric case $\tau_\Gamma \equiv \tau_1 = \tau_2$ where the memory kernel Eq. (3) reduces to a single exponential. For fixed barrier height $\beta U_0 = 3$ one only has two parameters, namely the inertial time τ_m/τ_D and the memory time τ_Γ/τ_D, both rescaled by the diffusion time τ_D. The dependence of the MFPT on βU_0 has previously been considered [36], and for the present case is discussed in Appendix G. In Fig. 4 (a) we show MFPTs from simulations for various fixed values of τ_Γ/τ_D as a function of τ_m/τ_D. As can be most clearly seen for the $\tau_\Gamma/\tau_D = 1$ data, for $\tau_m/\tau_D \ll 1$ the MFPT $\tau_{\mathrm{MFP}}/\tau_D$ becomes independent of τ_m/τ_D; this is the classical Kramers high-friction regime where $\tau_{\mathrm{MFP}} \sim \gamma$ [1, 47]. In the opposite limit $\tau_m/\tau_D \gg 1$, the MFPT scales as $\tau_{\mathrm{MFP}} \sim m/\gamma$, indicating the Kramers low-friction (energy diffusion) limit [1, 47]. In Fig. 4 (b) we show simulated MFPTs for various fixed values of τ_m/τ_D as a function of τ_Γ/τ_D. While for long memory, $(\tau_\Gamma/\tau_D)^2 \gg \max\{1, \tau_m/\tau_D\}$, the MFPT scales as
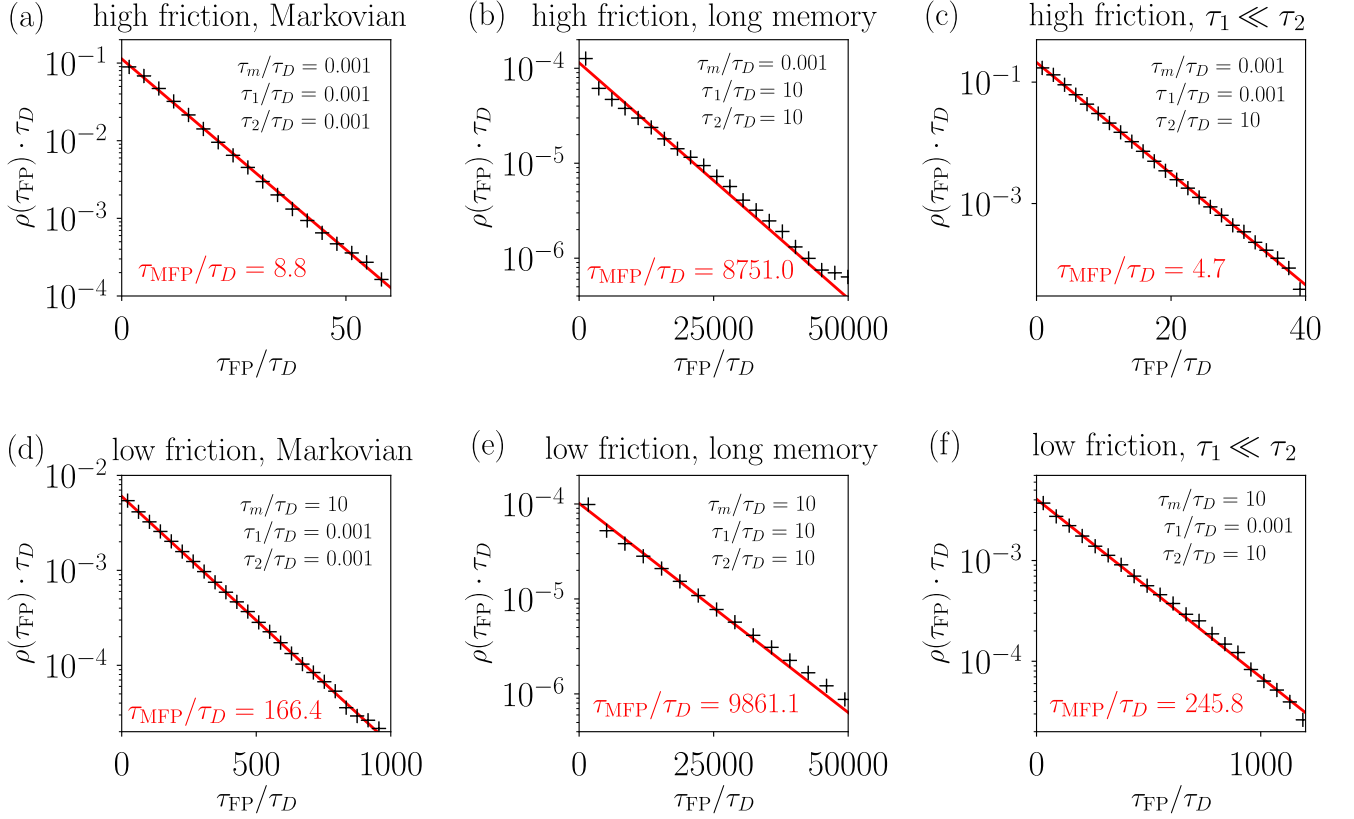
FIG. 3. First-passage time (FPT) distributions $\rho(\tau_{\mathrm{FP}})$ for barrier crossing from one potential well to the other. Simulation parameters are given in the legends. For each subplot, first-passage events are obtained from the numerical simulations as illustrated in Fig. 1 (b). The resulting normalized probability distribution $\rho(\tau_{\mathrm{FP}})$ is shown as black crosses. The MFPT value τ_{MFP} given in the plots is obtained by averaging over all first-passage events, and used to plot an exponential distribution as defined in Eq. (5), shown as a solid line.

$\tau_{\mathrm{MFP}} \sim \tau_\Gamma^2$ [31, 36], in the Markovian regime $\tau_\Gamma/\tau_D \ll 1$ the MFPT is independent of τ_Γ/τ_D. For high friction $\tau_m/\tau_D \ll 1$, an intermediate regime where memory accelerates barrier crossing compared to the Markovian limit $\tau_\Gamma/\tau_D \ll 1$, centered around $\tau_\Gamma/\tau_D \approx 0.1$, can be observed [36]. We thus see that memory can in the high friction case either accelerate or slow down the barrier-crossing dynamics, depending on the memory time. For long memory the barrier-crossing time grows quadratically with the memory time both for high friction and low friction. This asymptotic regime is intriguing, as it demonstrates that memory modifies the barrier-crossing dynamics, and in particular the mean first-passage time τ_{MFP}, even when the memory time τ_Γ is much shorter than τ_{MFP}.

We now present a crossover formula for the MFPT for a general multi-exponential memory kernel,

$$\Gamma(t) = \sum_{i=1}^{N} \frac{\gamma_i}{\tau_i} \exp\left(-|t|/\tau_i\right) \tag{6}$$

parametrized by friction coefficients γ_i and memory times τ_i, and define the friction coefficient as $\gamma = \sum_{i=1}^{N} \gamma_i$.

Inspired by the linear dependence of the reaction time on friction in the overdamped limit [1] and the linear dependence of the reaction rate on the memory kernel in the energy-diffusion limit [32], we construct a heuristic crossover formula for the MFPT as

$$\tau_{\mathrm{MFP}} = \sum_{i=1}^{n} \tau_{\mathrm{OD}}^{(i)} + \left(\sum_{i=1}^{n} 1/\tau_{\mathrm{ED}}^{(i)}\right)^{-1}, \tag{7}$$

where the overdamped MFPT contribution $\tau_{\mathrm{OD}}^{(i)}$ and the energy-diffusion MFPT contribution $\tau_{\mathrm{ED}}^{(i)}$ are given by

$$\frac{\tau_{\mathrm{OD}}^{(i)}}{\tau_D} = \frac{\gamma_i}{\gamma} \frac{e^{\beta U_0}}{\beta U_0} \left[\frac{\pi}{2\sqrt{2}} \frac{1}{1 + 10\beta U_0 \tau_i/\tau_D} + \sqrt{\beta U_0 \frac{\tau_m}{\tau_D}}\right], \tag{8}$$

$$\frac{\tau_{\mathrm{ED}}^{(i)}}{\tau_D} = \frac{\gamma}{\gamma_i} \frac{e^{\beta U_0}}{\beta U_0} \left[\frac{\tau_m}{\tau_D} + 4\beta U_0 \left(\frac{\tau_i}{\tau_D}\right)^2 + \sqrt{\beta U_0 \frac{\tau_m}{\tau_D}}\right]. \tag{9}$$

The first sum in Eq. (7) reflects that in the memoryless high-friction scenario the MFPT scales as $\tau_{\mathrm{MFP}} \sim \gamma =$
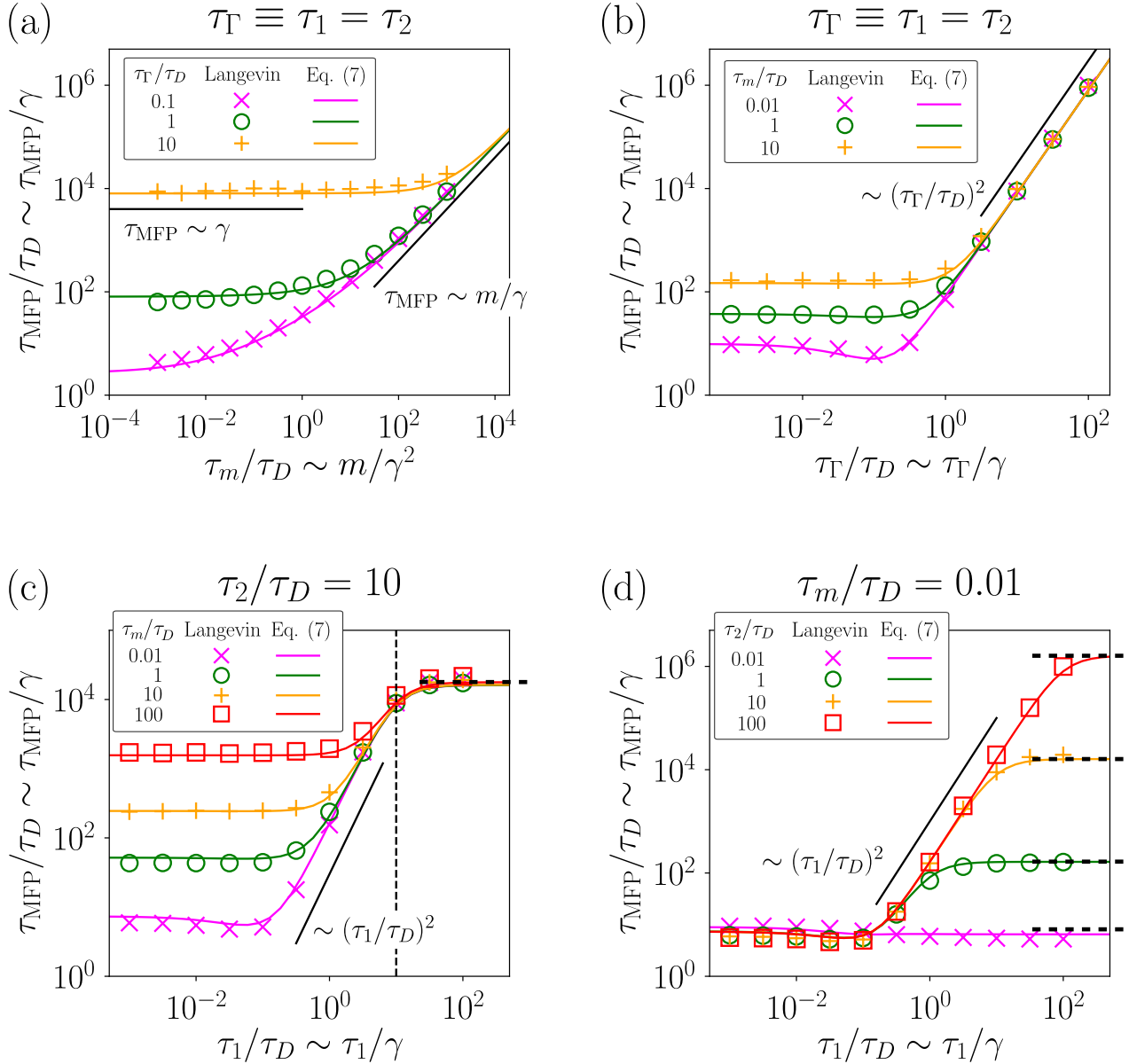
FIG. 4. Throughout the figure, colored symbols denote MFPT simulation results and colored lines represent the crossover formula Eq. (7), the barrier height is fixed at $\beta U_0 = 3$. (a), (b) MFPT results for single-exponential memory, i.e., for $\tau_\Gamma \equiv \tau_1 = \tau_2$. (a) The rescaled MFPT $\tau_{\mathrm{MFP}}/\tau_D$ is shown as a function of the rescaled inertial time τ_m/τ_D for several values of the rescaled memory time τ_Γ/τ_D. The asymptotic power law scalings $\tau_{\mathrm{MFP}}/\tau_D \sim \tau_m/\tau_D$ (Markovian low-friction regime) and $\tau_{\mathrm{MFP}}/\tau_D \equiv$ const. (Markovian high-friction regime) are shown as black bars. (b) The rescaled MFPT $\tau_{\mathrm{MFP}}/\tau_D$ is shown as a function of τ_Γ/τ_D for several values of τ_m/τ_D. The asymptotic power law scaling $\tau_{\mathrm{MFP}}/\tau_D \sim (\tau_\Gamma/\tau_D)^2$ [31, 36] is shown as a black bar. (c) MFPT results for bi-exponential memory at fixed $\tau_2/\tau_D = 10$ as function of τ_1/τ_D for several fixed values of τ_m/τ_D. The value at which $\tau_1 = \tau_2$ is indicated by a vertical dashed line. The black bar indicates the intermediate scaling $\tau_{\mathrm{MFP}}/\tau_D \sim (\tau_1/\tau_D)^2$, the horizontal dashed black line to the right denotes the prediction from Eq. (7) in the limit $\gamma_1 = 0$. (d) MFPT results for bi-exponential memory at fixed $\tau_m/\tau_D = 0.01$ as function of τ_1/τ_D for several values of τ_2/τ_D. The black bar indicates the intermediate scaling $\tau_{\mathrm{MFP}}/\tau_D \sim (\tau_1/\tau_D)^2$, the horizontal dashed black lines to the right denote the predictions from Eq. (7) in the limit $\gamma_1 = 0$.

$\sum_i \gamma_i$, as follows from the Kramers theory in the high-friction limit [1]. The inverse additivity of the individual MFPT contributions in the energy-diffusion regime, the second sum in Eq. (7), is derived in Appendix D. The ad-

ditivity of the overdamped- and energy-diffusion MFPT contributions in Eq. (7) was previously used to construct similar crossover formulas [48–50]. Our crossover formula for the MFPT obeys an important symmetry: In the

case of single-exponential memory, i.e. if all τ_i are equal, Eq. (7) only depends on the γ_i only via their sum γ, as it should. In this limit our expression slightly deviates from our previous single-exponential crossover formula [36]: First, the prefactor $\pi/(2\sqrt{2}) \approx 1.11$ in Eq. (8) replaces a factor 1 in Ref. [36], so that Eq. (8) reproduces the overdamped Kramers limit $\tau_m/\tau_D \ll 1$, $\tau_\Gamma/\tau_D \ll 1$ [1] exactly. Second, the prefactor 4 in the second term in Eq. (9) replaces a factor $e \approx 2.72$ in Ref. [36], which leads to improved matching with simulated MFPTs in the long-memory regime $(\tau_\Gamma/\tau_D)^2 \gg \max\{1, \tau_m/\tau_D\}$.

Equation (7) is in Fig. 4 (a), (b) included as colored solid lines and agrees with the numerical data very well. In particular, it reproduces all asymptotic scaling regimes of the single-exponential scenario, namely: i) the memoryless high-friction Kramers regime $\tau_\Gamma/\tau_D \ll 1$ and $\tau_m/\tau_D \ll 1$, given by the first term in Eq. (8) for $\tau_\Gamma/\tau_D = 0$ and observed for $\tau_m/\tau_D \ll 1$ in Fig. 4 (a); ii) the memoryless low-friction regime $\tau_\Gamma/\tau_D \ll 1$ and $\tau_m/\tau_D \gg 1$, given by the first term in Eq. (9) and observed for $\tau_m/\tau_D \gg 1$ in Fig. 4 (a); iii) the long-memory regime $(\tau_\Gamma/\tau_D)^2 \gg \max\{1, \tau_m/\tau_D\}$, given by the second term in Eq. (9) and observed for $\tau_\Gamma/\tau_D \gg 1$ in Fig. 4 (b). The last terms in Eqs. (8) and (9) are included to improve the crossover between the overdamped and energy-diffusion regimes and are fitted to the simulation MFPT data.

In Appendix G, Fig. 11 (a), we compare the crossover formula Eq. (7) with simulation results for varying βU_0 in the symmetric case $\tau_1 = \tau_2$; there, we find good agreement between the crossover formula and numerical results for $\beta U_0 \gtrsim 2$.

V. MFPT RESULTS FOR BI-EXPONENTIAL MEMORY

In Fig. 4 (c), (d) we compare simulation results for τ_{MFP} with the crossover formula Eq. (7) for the asymmetric scenario where the bi-exponential memory times τ_1 and τ_2 are unequal. Figure 4 (c) shows $\tau_{\mathrm{MFP}}/\tau_D$ as function of τ_1/τ_D for fixed $\tau_2/\tau_D = 10$ and several values of τ_m/τ_D. Throughout Fig. 4 (c) the crossover formula Eq. (7), denoted by colored solid lines, describes the simulation results very well. We see that for $\tau_1 \ll \tau_2$, i.e. to the left of the vertical dashed line that denotes $\tau_1 = \tau_2$, the MFPT behaves very similarly to the single-exponential MFPT results shown in Fig. 4 (b). As $\tau_1 \gtrsim \tau_2$, i.e. to the right of the vertical dashed line, the MFPT becomes independent of τ_1 and takes on the value which is obtained in the absence of the more slowly decaying exponential memory component, as indicated by the horizontal dashed black line which follows from Eq. (7) by taking the limit $\gamma_1 = 0$. In agreement with the behavior of the particle trajectories and the FPT distributions discussed before, the MFPT only depends on the shorter of the two memory times if at least one of the two memory times τ_1, τ_2 is larger than τ_D.

Figure 4 (d) shows $\tau_{\mathrm{MFP}}/\tau_D$ as function of τ_1/τ_D for fixed $\tau_m/\tau_D = 10$ and several values of τ_2/τ_D as indicated in the legend. Also in this plot, the crossover formula Eq. (7) describes the simulation data very accurately. For $\tau_1 \ll \tau_2$ we again obtain behavior reminiscent of the single-exponential results shown in Fig. 4 (b). As $\tau_1 \gtrsim \tau_2$ and $\tau_1 > \tau_D$, $\tau_{\mathrm{MFP}}/\tau_D$ saturates at a value that only depends on τ_m/τ_D and τ_2/τ_D, while the value of τ_1 becomes irrelevant. The horizontal dashed black lines to the right of the figure denote the predictions from Eq. (7) in the limit $\gamma_1 = 0$. For $\tau_2/\tau_D = 0.01$ (magenta crosses), Fig. 4 (d) contains no regime where $\tau_D < \tau_1 \ll \tau_2$, so that τ_{MFP} is almost independent of τ_1/τ_D throughout.

In Appendix F we compare our crossover formula to simulation data for a wider range of the parameters τ_m/τ_D, τ_1/τ_D, τ_2/τ_D at barrier height $\beta U_0 = 3$, confirming that Eq. (7) globally describes bi-exponential barrier crossing very well and that τ_{MFP} is dominated by the shorter memory time for all parameter values. In Appendix G we show that our crossover formula Eq. (7) agrees with simulations also for larger barrier heights βU_0. As demonstrated in Appendix E, Grote-Hynes (GH) theory [29] only describes the simulation data in the triple-limit of high-friction $\tau_m/\tau_D \ll 1$ and short memory $\tau_1/\tau_D \ll 1$, $\tau_2/\tau_D \ll 1$, which is why we do not compare our results with predictions of GH theory in the main text.

The dependence of the MFPT on the memory times τ_1 and τ_2 is summarized in Fig. 5 in terms of scaling diagrams for both high and low friction. For high friction, $\tau_m/\tau_D = 0.01$, we see in Fig. 5 (a) that the Markovian high-friction regime, which corresponds to the Kramers high-friction regime where $\tau_{\mathrm{MFP}} \sim \gamma$ [1], is obtained when both τ_1/τ_D and τ_2/τ_D become small. For $\tau_1/\tau_D > 1$ and $\tau_2/\tau_D > 1$ the memory slowdown regime is reached where the MFPT increases quadratically with the memory time. This regime is divided along the diagonal, since the shorter memory time dominates the barrier-crossing kinetics, such that for $\tau_1 > \tau_2$ one finds $\tau_{\mathrm{MFP}} \sim \tau_2^2$ while for $\tau_1 < \tau_2$ one finds $\tau_{\mathrm{MFP}} \sim \tau_1^2$. The Markovian and memory slowdown asymptotic regimes are separated by an intermediate memory speedup regime, where barrier crossing is slightly accelerated by the presence of memory as compared to the Markovian limit. Along the diagonal $\tau_1 = \tau_2$, the intermediate memory speedup and the asymptotic memory slowdown regimes are illustrated in Fig. 4 (b); parallel to the τ_1-axis, the memory speedup is illustrated in Fig. 5 (c) by a plot of τ_{MFP} for constant $\tau_2/\tau_D = 10^{-4}$.

For low friction, $\tau_m/\tau_D = 10$, shown in Fig. 5 (b), the Markovian regime is obtained for $\tau_1/\tau_D < 1$ and $\tau_2/\tau_D < 1$. For $\tau_1/\tau_D \gg \max\{1, \sqrt{\tau_m/\tau_D}\} = \sqrt{10}$ and $\tau_2/\tau_D \gg \max\{1, \sqrt{\tau_m/\tau_D}\} = \sqrt{10}$ the memory slowdown regime is reached where $\tau_{\mathrm{MFP}} \sim \tau_2^2$ or $\tau_{\mathrm{MFP}} \sim \tau_1^2$, depending on which memory time is smaller. In between these two asymptotic regimes, we find an intermediate regime where the barrier crossing is slowed down compared to the Markovian limit but the MFPT does not

display the quadratic memory-time dependence, which is illustrated in Fig. 5 (d) by a plot of τ_{MFP} for constant $\tau_2/\tau_D = 10^{-4}$. A plot of τ_{MFP} along the diagonal for $\tau_1 = \tau_2$ is shown in Fig. 4 (b).

There are different levels on which one can rationalize and intuitively understand the main result obtained here, namely that it is the memory contribution with the shorter decay time that dominates the barrier-crossing kinetics in the non-Markovian limit. On a formal level, the linear pole analysis of the positional autocorrelation function in Appendix C shows that for $\tau_D < \tau_1 \ll \tau_2$, the memory contribution that depends on τ_2 can be neglected, so that the particle motion only depends on τ_1.

An alternative viewpoint is obtained by mapping of the non-Markovian one-dimensional Langevin equation onto a system of N coupled Markovian degrees of freedom, see Appendix B. In this picture, each exponential contribution to the memory function $\Gamma(t)$ can be viewed as an independent heat bath with relaxation time τ_i, with which the particle exchanges energy, see Appendix B. Accordingly, the inverse additivity of the MF-PTs of each exponential memory contribution in the energy-diffusion regime, represented by the second term in Eq. (7), means that τ_{MFP} is dominated by the heat bath with the shortest relaxation time, i.e. by the heat bath which is the fastest in providing the particle with the energy needed for barrier crossing, which (for identical γ_i) is the heat bath with the smallest τ_i. In conclusion, for bi-exponential memory, the shorter of the two memory times dominates the barrier-crossing time simply because it provides the barrier-crossing energy faster.

Yet another way of understanding the dominance of the memory contribution with the shorter decay time is obtained by considering the memory integral in Eq. (1) for a bi-exponential kernel given by Eq. (3). The particle will undergo many oscillations (for low friction) or random fluctuations (for high friction) within a well before attempting to cross the barrier. If the memory times are longer than the intrinsic relaxation time of the particle (which can be the intrinsic diffusion time τ_D or the oscillation period depending on whether one is in the high-friction or the low-friction regime), the convolution of the particle velocity history with the exponential memory contribution with the longer memory time will give a smaller friction contribution than the convolution with the exponential memory contribution with the shorter memory time (again assuming equal memory amplitudes γ_1 and γ_2), simply because the mean of the particle velocity is zero. This shows directly that memory effects in confinement tend to be dominated by the shorter memory contributions.

VI. FREE DIFFUSION CASE

While barrier-crossing dynamics is dominated by the memory contribution with the shorter memory time in the non-Markovian limit, in the absence of an external potential, i.e. for $U(x) = 0$, the long-time diffusive behavior is always expected to be determined by the total friction $\gamma = \gamma_1 + \gamma_2$. In Fig. 6 we show mean-squared displacements (MSDs)

$$\langle \Delta x^2(t) \rangle = \left\langle [x(t) - x(0)]^2 \right\rangle \qquad (10)$$

obtained from simulations without an external potential, $U(x) = 0$, and unequal memory times $\tau_1/\tau_D = 0.001$, $\tau_2/\tau_D = 10$, as blue dashed lines. These parameters used are the same as in Fig. 2 (c), (f). Figure 6 (a) shows the high-friction scenario $\tau_m/\tau_D = 0.001$. For times $t \gg \tau_2$ the MSD is well described by

$$\langle \Delta x^2(t) \rangle = 2\frac{1}{\beta\gamma}t = 2Dt, \qquad (11)$$

which in Fig. 6 (a) is denoted by a green solid line, and which is the expected result for the MSD of a Brownian particle with friction coefficient γ and where we used the Einstein relation to define the diffusion constant as $D = 1/(\beta\gamma)$. For shorter times $\tau_1 < t < \tau_2$, only the shorter memory contribution, characterized by τ_1, contributes to the friction and the simulated MSD is well described by

$$\langle \Delta x^2(t) \rangle = 2\frac{1}{\beta\gamma_1}t = 4Dt, \qquad (12)$$

which in Fig. 6 (a) is denoted by an orange solid line.

For the low-friction scenario $\tau_m/\tau_D = 10$ depicted in Fig. 6 (b), the inertial regime where $\langle \Delta x^2(t) \rangle \sim t^2/(m\beta)$ appears for $t \ll \tau_m$. For $t \gtrsim \tau_m$ the MSD exhibits diffusive behavior determined by the full friction coefficient γ, i.e. $\langle \Delta x^2(t) \rangle = 2t/(\beta\gamma) = 2Dt$, since for $t \gg \tau_m$ we simultaneously fulfill $t \gg \tau_1$ and $t \gg \tau_2$.

We conclude that while barrier-crossing kinetics is completely dominated by the shorter memory time if the particle relaxation time is shorter than the longer memory time, the long-time free diffusion behavior in the presence of bi-exponential memory is determined by the sum of both exponential memory contributions. This simply reflects that the particle relaxation time diverges in the free-diffusion scenario.

VII. CONCLUSIONS

Our Langevin simulations in the presence of a bi-exponential memory function show that if at least one of the two memory times τ_1, τ_2 is larger than τ_D, then the barrier-crossing time τ_{MFP} is dominated by the shorter of the two memory times. The simulation results are obtained for the restricted case where the exponential memory contributions have the same integral weight. Based on asymptotic matching and symmetry considerations, we construct a crossover formula for τ_{MFP} which describes our simulation results for all parameters very well. This formula applies to general multi-exponential memory function with arbitrary weights and decay times and
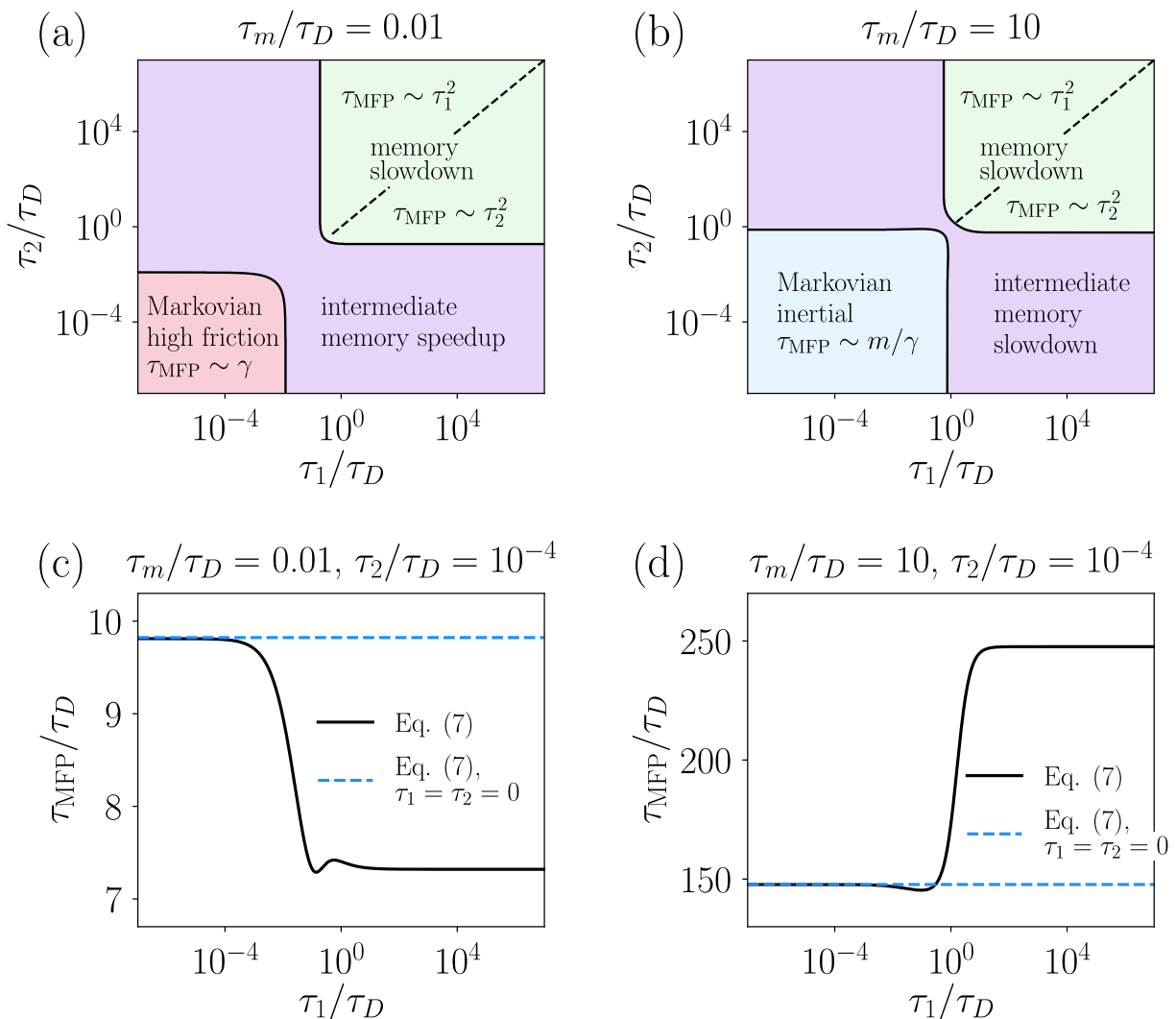
FIG. 5. (a), (b) Scaling diagrams for the dependence of the MFPT τ_{MFP} on the rescaled memory times τ_1/τ_D and τ_2/τ_D for (a) high friction $\tau_m/\tau_D = 0.01$ and (b) low friction $\tau_m/\tau_D = 10$. In (a), the transition from the Markovian high-friction regime to the intermediate memory speedup regime is defined by the location where τ_{MFP} is smaller by 10% than the Markovian limit $\tau_1 = \tau_2 = 0$ (based on the crossover formula Eq. (7)). The transition from the intermediate memory speedup regime to the asymptotic memory slowdown regime is defined by the location where τ_{MFP} equals the Markovian limit. In (b), the transition from the Markovian low-friction regime to the intermediate memory slowdown regime is defined by the location where τ_{MFP} is larger by 10% than the Markovian limit $\tau_1 = \tau_2 = 0$ (based on the crossover formula Eq. (7)). The transition from the intermediate memory slowdown regime to the asymptotic memory slowdown regime is defined by the location where τ_{MFP} is twice as large as in the Markovian limit. The dashed diagonal lines in (a) and (b) in the asymptotic memory slowdown regime indicate the crossover from τ_1-dominated barrier crossing for $\tau_1 \ll \tau_2$, to τ_2-dominated barrier crossing for $\tau_2 \ll \tau_1$. (c), (d) The rescaled MFPT $\tau_{\mathrm{MFP}}/\tau_D$ according to Eq. (7) is shown as a function of τ_1/τ_D for fixed $\tau_2/\tau_D = 10^{-4}$ and (a) $\tau_m/\tau_D = 0.01$, and (b) $\tau_m/\tau_D = 10$. The dashed line denotes the Markovian limit, obtained from Eq. (7) by setting $\tau_1 = \tau_2 = 0$. All data is obtained for a fixed barrier height of $\beta U_0 = 3$.

corroborates that the shortest memory time is expected to dominate τ_{MFP} in the non-Markovian limit.

Our results have a number of important consequences: Usually it is assumed that the slow degrees of freedom of a system dominate rare events and in particular the MFPT τ_{MFP}; for the case of barrier crossing in the presence of memory functions with different time scales, our results show that this time scale separation principle is violated. Our findings suggest that instead of keeping only the slowest degrees of freedom, which is conventionally done in coarse graining procedures, one also needs to keep the fastest orthogonal degrees of freedom if non-Markovian effects are important. Of course, the choice of the degrees of freedom that should be included requires good understanding of all relevant time scales.
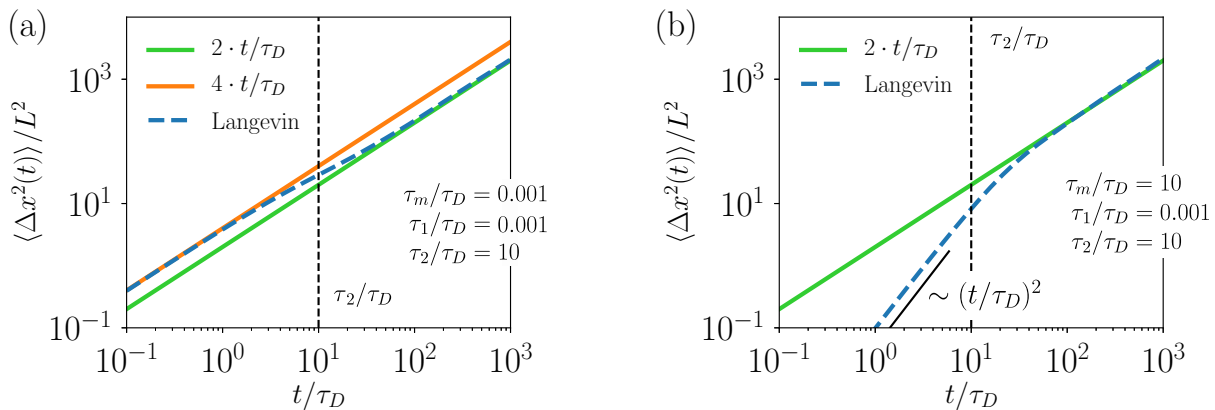
Non-Markovian effects have been demonstrated to be

FIG. 6. Comparison of the simulated mean-squared displacement (MSD), shown as dashed blue line (consisting of 8 data points per decade), with asymptotic predictions in the absence of an external potential for $U(x) = 0$. (a) Results for high friction $\tau_m/\tau_D = 0.001$ and memory times $\tau_1/\tau_D = 0.001$ and $\tau_2/\tau_D = 10$, the same parameters as used in Fig. 2 (c). The solid lines denote the expected MSD for diffusion with friction coefficients $\gamma/2$ (orange line) and γ (green line). The vertical dashed line denotes τ_2/τ_D. (b) Results for low friction $\tau_m/\tau_D = 10$ and memory times $\tau_1/\tau_D = 0.001$ and $\tau_2/\tau_D = 10$, the same parameters as used in Fig. 2 (f). The solid green line denotes the expected MSD for diffusion with friction coefficient γ. The black bar indicates the power law $\langle \Delta x^2(t) \rangle \sim t^2$ expected for ballistic motion, the vertical dashed line denotes τ_2/τ_D. Note that for free diffusion there exist analytical expressions for both the Laplace- and Fourier-transform of the MSD [51, 52], so that Fig. 6 could have been generated without invoking numerical simulations.

important for fast molecular transition such as the dihedral barrier dynamics of butane in solvents [15, 16]. The effect of the different memory times of the multi-scale memory kernel that have been extracted from simulations will have to be examined in future work. Likewise, protein dynamics has been suggested to be subject to memory effects in a number of works [27, 28]. Here our crossover formula Eq. (7) will be useful, because it fills the gap between theoretical works on non-Markovian barrier crossing, which are typically confined to single-exponential memory [31, 33, 34], and real physical systems, where orthogonal degrees of freedom typically feature several relaxation time scales [12, 15, 16, 18, 19, 37, 38]. Another field of application are chemical reactions in solvents, such as proton transfer reactions in water [43, 53]. In such reactions, the friction is presumably rather small, such that the low-friction regime, characterized by $\tau_m/\tau_D > 1$, is relevant. But also in the low-friction limit, our results show that for multi-scale memory the smaller memory time becomes dominant in the non-Markovian limit.

Appendix A: Dimensionless form of the GLE

We consider the one-dimensional generalized Langevin equation

$$m\,\ddot{x}(t) = -\int_0^t \Gamma(t - t')\dot{x}(t')\,\mathrm{d}t' - U'(x(t)) + \eta(t), \quad \text{(A1)}$$

where m is the mass of the particle, x its position, $\Gamma(t)$ the memory kernel and $U'(x)$ denotes the derivative of the external potential $U(x)$. The random force $\eta(t)$ is Gaussian with zero mean, $\langle \eta(t) \rangle = 0$, and obeys the generalized fluctuation-dissipation theorem (FDT)

$$\beta \langle \eta(t)\eta(t') \rangle = \Gamma(|t - t'|). \quad \text{(A2)}$$

We consider a multi-exponential memory kernel with friction coefficients γ_i and memory times τ_i,

$$\Gamma(t) = \sum_{i=1}^{N} \frac{\gamma_i}{\tau_i} e^{-|t|/\tau_i}, \quad \text{(A3)}$$

and define the total friction $\gamma := \sum_{i=1}^{N} \gamma_i$. Defining a dimensionless position $\tilde{x} = x/L$ and a rescaled time $t = \tilde{t}\tau_D$ and multiplying Eq. (A1) by βL, we obtain

$$\frac{\tau_m}{\tau_D}\ddot{\tilde{x}}(\tilde{t}) = -\sum_{i=1}^{N}\frac{\gamma_i}{\gamma}\frac{\tau_D}{\tau_i}\int_0^{\tilde{t}}\mathrm{d}\tilde{t}'\exp\left[-\frac{\tau_D}{\tau_i}\left(\tilde{t}-\tilde{t}'\right)\right]\dot{\tilde{x}}(\tilde{t}') + \tilde{F}\left(\tilde{x}(\tilde{t})\right) + \tilde{\eta}(\tilde{t}), \tag{A4}$$

where $\tilde{F}(\tilde{x}) := \beta L\partial_x U(L\tilde{x}) \equiv \beta LU'(L\tilde{x})$ and $\tilde{\eta}(\tilde{t}) := \beta L\,\eta(\tau_D\tilde{t})$. Using Eq. (A2), it follows that the autocorrelation of the dimensionless random force is given by

$$\langle\tilde{\eta}(\tilde{t})\tilde{\eta}(\tilde{t}')\rangle = \sum_{i=1}^{N}\frac{\gamma_i}{\gamma}\frac{\tau_D}{\tau_i}\exp\left[-\frac{\tau_D}{\tau_i}|\tilde{t}-\tilde{t}'|\right]. \tag{A5}$$

For $N = 1$ we recover the case of single-exponential memory, for $N = 2$ and $\gamma_1 = \gamma_2$ we obtain the symmetric bi-exponential system that we considered in the simulations. For given potential U, Eqs. (A4), (A5), are fully determined by the dimensionless ratios τ_m/τ_D, τ_i/τ_D, γ_i/γ.

Appendix B: Transforming the GLE into a coupled system of Markovian equations

We now show that the dimensionless GLE with multi-exponential memory, Eqs. (A4), (A5), is equivalent to the Markovian coupled system of equations

$$m\ddot{x} = -\partial_x V, \tag{B1}$$
$$0 = -\gamma_i\dot{y}_i - \partial_i V + \xi_i, \qquad i \in \{1,...,N\}, \tag{B2}$$

where the ξ_i are Markovian Gaussian random fields with zero mean and variance

$$\beta\langle\xi_i(t)\xi_j(t)\rangle = 2\gamma_i\delta_{i,j}\delta(t-t'), \qquad i,j \in \{1,...,N\}, \tag{B3}$$

the potential V is given by

$$V(x, y_1, ..., y_N) = U(x) + \sum_{j=1}^{N}\frac{k_j}{2}(y_j - x)^2, \tag{B4}$$

and $\partial_i V$ denotes the partial derivative of V w.r.t. y_i.

Defining dimensionless positions $\tilde{x}(\tilde{t}) := x(\tau_D\tilde{t})/L$, $\tilde{y}_i(\tilde{t}) := y_i(\tau_D\tilde{t})/L$, inserting the potential Eq. (B4) in Eqs. (B1), (B2), introducing a rescaled time variable $t = \tilde{t}\tau_D$, and multiplying by βL, we obtain

$$\frac{\tau_m}{\tau_D}\ddot{\tilde{x}}(\tilde{t}) = \tilde{F}\left(\tilde{x}(\tilde{t})\right) + \sum_{i=1}^{N}\frac{\tau_D}{\tau_i}\frac{\gamma_i}{\gamma}\left[\tilde{y}_i(\tilde{t}) - \tilde{x}(\tilde{t})\right], \tag{B5}$$

$$\dot{\tilde{y}}_i(\tilde{t}) = -\frac{\tau_D}{\tau_i}\tilde{y}_i(\tilde{t}) + \frac{\tau_D}{\tau_i}\tilde{x}(\tilde{t}) + \sqrt{\frac{\gamma}{\gamma_i}}\tilde{\xi}_i(\tilde{t}) \quad 1 \le i \le N, \tag{B6}$$

where $\tilde{F}(\tilde{x}) := -\beta L\partial_x U(L\tilde{x}) \equiv \beta LU'(L\tilde{x})$, $\tau_i := \gamma_i/k_i$, and the correlators of the dimensionless random forces $\tilde{\xi}(\tilde{t}) := \beta L\sqrt{\gamma/\gamma_i}\xi(\tau_D\tilde{t})$ are given by

$$\left\langle\tilde{\xi}_i(\tilde{t})\tilde{\xi}_j(\tilde{t})\right\rangle = 2\delta_{i,j}\delta(\tilde{t}-\tilde{t}') \qquad i,j \in \{1,...,N\}. \tag{B7}$$

To show the equivalence of Eqs. (B5), (B6), (B7) to the GLE Eq. (A4), (A5), we first note that the solution to Eq. (B6) is given by

$$\tilde{y}_i(\tilde{t}) = \tilde{y}_i(0)\exp\left(-\frac{\tau_D}{\tau_i}\tilde{t}\right)$$
$$+ \frac{\tau_D}{\tau_i}\int_0^{\tilde{t}}\mathrm{d}\tilde{t}'\exp\left[-\frac{\tau_D}{\tau_i}(\tilde{t}-\tilde{t}')\right]\tilde{x}(\tilde{t}') \tag{B8}$$
$$+ \sqrt{\frac{\gamma}{\gamma_i}}\int_0^{\tilde{t}}\mathrm{d}\tilde{t}'\exp\left[-\frac{\tau_D}{\tau_i}(\tilde{t}-\tilde{t}')\right]\tilde{\xi}_i(\tilde{t}').$$

Using integration by parts on the second term of this expression and inserting the result into Eq. (B5), we obtain

$$\frac{\tau_m}{\tau_D}\ddot{\tilde{x}}(\tilde{t}) = -\sum_{i=1}^{N}\frac{\gamma_i}{\gamma}\frac{\tau_D}{\tau_i}\int_0^{\tilde{t}}\mathrm{d}\tilde{t}'\exp\left[-\frac{\tau_D}{\tau_i}\left(\tilde{t}-\tilde{t}'\right)\right]\dot{\tilde{x}}(\tilde{t}') + \tilde{F}(\tilde{x}(\tilde{t})) + \tilde{\eta}_R(\tilde{t}), \tag{B9}$$

where we define

$$\tilde{\eta}_R(\tilde{t}) = \sum_{i=1}^{N}\left\{\frac{\gamma_i}{\gamma}\frac{\tau_D}{\tau_i}[\tilde{y}_i(0) - \tilde{x}(0)]\exp\left[-\frac{\tau_D}{\tau_i}\left(\tilde{t}\right)\right]\right.$$
$$\tag{B10}$$
$$\left.+ \sqrt{\frac{\gamma_i}{\gamma}}\frac{\tau_D}{\tau_i}\int_0^{\tilde{t}}\mathrm{d}\tilde{t}'\exp\left[-\frac{\tau_D}{\tau_i}(\tilde{t}-\tilde{t}')\right]\tilde{\xi}_i(\tilde{t}')\right\}.$$

To obtain the equivalence of Eq. (B9) to Eq. (A4), $\tilde{\eta}_R$ needs to be a stochastic processes identi-cal to $\tilde{\eta}$. For this, we assume that, for given $x(0)$, the $y_i(0)$ are distributed according to a Boltzmann distribution $\rho(y_1(0),...,y_N(0)\,|\,x(0)) \sim \exp\left[-\beta V(x(0), y_1(0),...,y_N(0))\right]$, which using Eq. (B4) leads to normally distributed $\tilde{y}_i(0) - \tilde{x}(0)$ with zero mean and covariance matrix

$$\langle[\tilde{y}_i(0) - \tilde{x}(0)][\tilde{y}_j(0) - \tilde{x}(0)]\rangle = \delta_{i,j}\left(\frac{\gamma_i}{\gamma}\frac{\tau_D}{\tau_i}\right)^{-1}. \tag{B11}$$

With this, the mean of $\tilde{\eta}_R$ is easily seen to be zero, and the variance is given by

$$\langle \tilde{\eta}_R(\tilde{t})\tilde{\eta}_R(\tilde{t}')\rangle = \sum_{i=1}^{N} \left(\frac{\gamma_i}{\gamma}\frac{\tau_D}{\tau_i}\right)^2 \exp\left[-\frac{\tau_D}{\tau_i}(\tilde{t}+\tilde{t}')\right] \left\langle(\tilde{y}_i(0)-\tilde{x}(0))^2\right\rangle \tag{B12}$$

$$+ \sum_{i=1}^{N} \frac{\gamma_i}{\gamma}\left(\frac{\tau_D}{\tau_i}\right)^2 \int_0^{\tilde{t}} du \int_0^{\tilde{t}'} du' \exp\left[-\frac{\tau_D}{\tau_i}(\tilde{t}+\tilde{t}'-u-u')\right] \langle\tilde{\xi}_i(u)\tilde{\xi}_i(u')\rangle$$

$$= \sum_{i=1}^{N} \exp\left[-\frac{\tau_D}{\tau_i}(\tilde{t}+\tilde{t}')\right]\frac{\gamma_i}{\gamma}\frac{\tau_D}{\tau_i}$$

$$+ \sum_{i=1}^{N} 2\frac{\gamma_i}{\gamma}\left(\frac{\tau_D}{\tau_i}\right)^2 \int_0^{\min\{\tilde{t},\tilde{t}'\}} du \exp\left[-\frac{\tau_D}{\tau_i}(\tilde{t}+\tilde{t}'-2u)\right] \tag{B13}$$

$$= \sum_{i=1}^{N} \exp\left[-\frac{\tau_D}{\tau_i}(\tilde{t}+\tilde{t}')\right]\frac{\gamma_i}{\gamma}\frac{\tau_D}{\tau_i}$$

$$+ \sum_{i=1}^{N} \frac{\gamma_i}{\gamma}\frac{\tau_D}{\tau_i}\left\{\exp\left[-\frac{\tau_D}{\tau_i}\left(\tilde{t}+\tilde{t}'-2\min\{\tilde{t},\tilde{t}'\}\right)\right]-\exp\left[-\frac{\tau_D}{\tau_i}\left(\tilde{t}+\tilde{t}'\right)\right]\right\} \tag{B14}$$

$$= \sum_{i=1}^{N} \frac{\gamma_i}{\gamma}\frac{\tau_D}{\tau_i}\exp\left[-\frac{\tau_D}{\tau_i}|\tilde{t}-\tilde{t}'|\right], \tag{B15}$$

where we use that $\tilde{t}+\tilde{t}'-2\min\{\tilde{t},\tilde{t}'\} = |\tilde{t}-\tilde{t}'|$. Thus, $\tilde{\eta}_R$ is a Gaussian stochastic process with the first two moments identical to those of the Gaussian stochastic process $\tilde{\eta}$, so that $\tilde{\eta}_R \equiv \tilde{\eta}$. For $N=2$ and $\gamma_1 = \gamma_2$, we obtain the system considered in the simulations in the main text.

To simulate Eqs. (B5), (B6) using a Runge-Kutta scheme, we introduce a further auxiliary variable z to rewrite the equations as a system of first-order equations

$$\dot{\tilde{x}}(\tilde{t}) = z(\tilde{t}), \tag{B16}$$

$$\frac{\tau_m}{\tau_D}\dot{z}(\tilde{t}) = \sum_{i=1}^{N} \frac{\tau_D}{\tau_i}\frac{\gamma_i}{\gamma}\left[\tilde{y}_j(\tilde{t})-\tilde{x}(\tilde{t})\right] + \tilde{F}\left(\tilde{x}(\tilde{t})\right), \tag{B17}$$

$$\dot{\tilde{y}}_i(\tilde{t}) = -\frac{\tau_D}{\tau_i}\left[\tilde{y}_i(\tilde{t})-\tilde{x}(\tilde{t})\right]+\sqrt{\frac{\gamma}{\gamma_i}}\tilde{\xi}_i(\tilde{t}) \quad 1\leq i\leq N, \tag{B18}$$

Note that the equivalence of Eqs. (B1), (B2), (B3), (B4) to Eqs. (A4), (A5), physically means that multi-exponential memory can be interpreted as the result of the interaction of a particle x with N independent reservoirs y_i with finite relaxation times τ_i.

Appendix C: Analysis of autocorrelation function

In Fig. 2 we observe similarities between the dynamics in the asymmetric bi-exponential scenario $\tau_1 \ll \tau_2$ and the single-exponential scenario characterized by the smaller memory time τ_1, indicating that the smaller memory time dominates the barrier-crossing kinetics. This can be rationalized by an asymptotic analysis of the

autocorrelation function $C(t) \equiv \langle x(t)x(0)\rangle$ that characterizes the particle motion within one potential well. The following calculation is a generalization of the analysis carried out for the single-exponential memory kernel in Ref. [36]. We consider the GLE (1) in a harmonic potential $U(x) \simeq Kx^2/2$ and for times $t \gg \tau_1, \tau_2$, so that we can replace the upper limit in the memory integral by infinity. Fourier transforming Eq. (1) and solving for $\tilde{x}(\omega)$ yields

$$\tilde{x}(\omega) = \frac{\tilde{\eta}(\omega)}{K - m\omega^2 + i\omega\tilde{\Gamma}_+(\omega)} \equiv \tilde{Q}(\omega)\tilde{\eta}(\omega), \tag{C1}$$

where the half-sided Fourier transform $\tilde{\Gamma}_+$ of the bi-exponential memory kernel $\Gamma(t)$ is given by

$$\tilde{\Gamma}_+(\omega) = \int_0^\infty dt\; e^{-i\omega t}\Gamma(t) = \frac{\gamma}{2}\sum_{j=1}^{2}\frac{1}{1+i\omega\tau_j}, \tag{C2}$$

while the full Fourier transform is

$$\tilde{\Gamma}(\omega) = \tilde{\Gamma}_+(\omega) + \tilde{\Gamma}_+(-\omega) = \gamma\sum_{j=1}^{2}\frac{1}{1+\omega^2\tau_j^2}. \tag{C3}$$

Using Eq. (C1), we calculate the autocorrelation func-

tion $C(t) \equiv \langle x(t)x(0) \rangle$ as

$$C(t) \equiv \langle x(t)x(0) \rangle = \int \frac{d\omega}{2\pi} e^{i\omega t} \int \frac{d\omega'}{2\pi} \langle \tilde{x}(\omega)\tilde{x}(\omega') \rangle \tag{C4}$$

$$= \int \frac{d\omega}{2\pi} e^{i\omega t} \int \frac{d\omega'}{2\pi} \tilde{Q}(\omega)\tilde{Q}(\omega') \langle \tilde{\eta}(\omega)\tilde{\eta}(\omega') \rangle \tag{C5}$$

$$= \beta^{-1} \int \frac{d\omega}{2\pi} e^{i\omega t} \int \frac{d\omega'}{2\pi} 2\pi\delta(\omega + \omega')\tilde{\Gamma}(\omega)\tilde{Q}(\omega)\tilde{Q}(\omega') \tag{C6}$$

$$= \beta^{-1} \int \frac{d\omega}{2\pi} e^{i\omega t} \tilde{\Gamma}(\omega)\tilde{Q}(\omega)\tilde{Q}(-\omega), \tag{C7}$$

where we used that the Fourier transform of the generalized FDT is $\langle \tilde{\eta}(\omega)\tilde{\eta}(\omega') \rangle = \beta^{-1} 2\pi\delta(\omega + \omega') \tilde{\Gamma}(\omega)$. Thus the Fourier transform of $C(t)$ is finally given by

$$\beta\tilde{C}(\omega) = \tilde{\Gamma}(\omega)\tilde{Q}(\omega)\tilde{Q}(-\omega) \tag{C8}$$

$$= \gamma \sum_{j=1}^{2} \left[\frac{1}{1 + \omega^2\tau_j^2} \frac{1}{K - m\omega^2 + i\omega\gamma/2 \sum_{k=1}^{2}(1 + i\omega\tau_k)^{-1}} \right.$$

$$\left. \times \frac{1}{K - m\omega^2 - i\omega\gamma/2 \sum_{l=1}^{2}(1 - i\omega\tau_l)^{-1}} \right] \tag{C9}$$

$$= \gamma \sum_{j=1}^{2} \left\{ (1 + \omega^2\tau_j^2) \left[(K - m\omega^2)^2 - \omega\gamma \sum_{k=1}^{2} \omega\tau_k(1 + \omega^2\tau_k^2)^{-1} \right. \right. \tag{C10}$$

$$\left. \left. + \frac{\omega^2\gamma^2}{4} \sum_{k,l=1}^{2} (1 + i\omega\tau_k)^{-1}(1 - i\omega\tau_l)^{-1} \right]^{-1} \right\}.$$

For τ_1, τ_2 large, we rewrite this as

$$\beta\tilde{C}(\omega) = \frac{\gamma}{\omega^2\tau_1^2} \left[(K - m\omega^2)^2 + \sum_{j=1}^{2} \mathcal{O}\left((\omega\tau_j)^{-1}\right) \right]^{-1}$$

$$+ \frac{\gamma}{\omega^2\tau_2^2} \left[(K - m\omega^2)^2 + \sum_{j=1}^{2} \mathcal{O}\left((\omega\tau_j)^{-1}\right) \right]^{-1}, \tag{C11}$$

so that to order $(\omega\tau_i)^2$ the autocorrelation function is just the sum of two terms corresponding to the two single-exponential memory contributions. For $\tau_1 \ll \tau_2$, the term involving τ_1 dominates and we obtain

$$\beta\tilde{C}(\omega) \approx \frac{\gamma}{\omega^2\tau_1^2} \left[(K - m\omega^2)^2 \right]^{-1}. \tag{C12}$$

The result is independent of τ_2, showing that the dynamics is indeed dominated by τ_1, which explains the behavior of the trajectories shown in Fig. 2 (c), (f).

Appendix D: Multi-exponential mean first-passage time in the energy diffusion regime

In the energy-diffusion limit and for high barriers, the barrier-crossing rate is given by [32]

$$k_{\text{ED}} = \frac{\beta\omega_0}{8\pi} e^{-\beta U_0} \int_{-\infty}^{\infty} dt \int_{-\infty}^{\infty} ds \, \Gamma(|t - s|)\dot{x}_0(t)\dot{x}_0(s), \tag{D1}$$

where $\omega_0 = \sqrt{U''(-L)/m}$ is the well frequency, and $\dot{x}_0$ is the velocity of the particle of the undamped system described by Eq. (1) without memory kernel Γ and random force η, starting at the barrier top with $\dot{x}_0(0) = 0^-$ and traversing the left well once [32]. Since Eq. (D1) is linear in Γ, for a multi-exponential kernel it immediately follows that

$$k_{\text{ED}} = \sum_i k_{\text{ED}}^{(i)}, \tag{D2}$$

where $k_{\text{ED}}^{(i)}$ is the single-exponential barrier-crossing rate corresponding the i-th exponential. From this and the relation $\tau_{\text{MFP}} \sim 1/k$ between MFPT τ_{MFP} and barrier-crossing rate k [36, 54], the second sum in Eq. (7) follows.

Appendix E: Comparison of numerical MFPTs to GH theory

In Fig. 7 we compare numerical MFPTs to Grote-Hynes (GH) theory [29]. Consistent with previous results [36], we find that GH theory only describes the numerical MFPTs in the high-friction regime $\tau_m/\tau_D \ll 1$ and if both memory times are small, $\tau_1/\tau_D, \tau_2/\tau_D \ll 1$. If either $\tau_m/\tau_D \gg 1$ or $\min\{\tau_1/\tau_D, \tau_2/\tau_D\} \gg 1$, then GH theory reduces to the transition state theory (TST) limit where $\tau_{\mathrm{MFP}}/\tau_D \sim \sqrt{\tau_m/\tau_D}$, as can be seen in Figs. 7 (d)-(f). Thus, also for bi-exponential memory GH theory only yields accurate results in the high-friction short-memory regime.

The disagreement between our Langevin results and GH theory is not surprising, since the latter is by construction not intended for the energy diffusion regime. More specifically, GH theory considers a GLE close to the barrier top, so that the theory does not include memory effects from the motion of the particle in the potential well; the GLE model we consider here has a global position-indepedent memory function [33]. Therefore, only in or close to the overdamped regime, where memory effects from motion in the well are not relevant to the dynamics close to the barrier top, do the predictions of GH theory and our numerical results agree.

Appendix F: Global comparison of numerical data to Eq. (7) at $\beta U_0 = 3$

In Figs. 8, 9, 10 we compare predictions of the crossover formula Eq. (7) for τ_{MFP} to numerical results. These figures, which we discuss in detail in the following paragraphs, show that Eq. (7) quantitively describes the bi-exponential MFPTs over the whole parameter range of τ_m/τ_D, τ_1/τ_D, τ_2/τ_D considered, and in particular that the MFPT is in the non-Markovian regime dominated by the shorter memory time.

Figure 8 shows $\tau_{\mathrm{MFP}}/\tau_D$ as function of τ_1/τ_D for fixed values of τ_m/τ_D, τ_2/τ_D. In the figure we see that for $\tau_1 \ll \tau_2$, i.e., to the left of the vertical dashed lines that denote $\tau_1 = \tau_2$, the MFPT behaves similar to the single-exponential MFPT shown in Fig. 4 (b). In particular, for $\tau_m/\tau_D = 0.01$ (magenta crosses) the memory acceleration regime can be seen in Fig. 8 (b), (c) for $\tau_1/\tau_D \approx 0.1$, followed by the power-law scaling $\tau_{\mathrm{MFP}}/\tau_D \sim (\tau_1/\tau_D)^2$ for $0.1 \lesssim \tau_1/\tau_D \lesssim \tau_2/\tau_D$. As $\tau_1 \gtrsim \tau_2$, i.e., to the right

of the vertical dashed lines, the MFPT becomes independent of τ_1. This can prominently be seen in Fig. 8 (a), where $\tau_2/\tau_D = 0.01$ is small and $\tau_{\mathrm{MFP}}/\tau_D$ is almost constant for $\tau_1 > \tau_2$. Throughout Fig. 8 the crossover formula Eq. (7) describes the numerical results very well.

Figure 9 shows $\tau_{\mathrm{MFP}}/\tau_D$ as function of τ_1/τ_D for fixed values of τ_2/τ_D, τ_m/τ_D. In Fig. 9 (a), we again see single-exponential behavior reminiscent of Fig. 4 (b). More explicitly, for $\tau_2/\tau_D = 1, 10, 100$, we observe a slight dip in $\tau_{\mathrm{MFP}}/\tau_D$ for $\tau_1/\tau_D \approx 0.1$, followed by power-law scaling $\tau_{\mathrm{MFP}}/\tau_D \sim (\tau_1/\tau_D)^2$ for $0.1 \lesssim \tau_1/\tau_D \lesssim \tau_2/\tau_D$. As $\tau_1 \gtrsim \tau_2$, $\tau_{\mathrm{MFP}}/\tau_D$ saturates to a value determined by τ_m/τ_D, τ_2/τ_D. For $\tau_2/\tau_D = 0.01$ (magenta crosses), Fig. 9 (a) contains no regime where $\tau_1 \ll \tau_2$, and $\tau_{\mathrm{MFP}}/\tau_D$ is almost independent of τ_1/τ_D throughout. Figs. 9 (b), (c) show similar behavior, and as expected from the single-exponential data for $\tau_m/\tau_D = 1, 10$ (see Fig. 4 (a)), a dip in the MFPT for $\tau_1/\tau_D \approx 0.1$ cannot be observed in the logarithmic representation of $\tau_{\mathrm{MFP}}/\tau_D$. Again, the crossover formula Eq. (7) describes the data very accurately throughout.

Figure 10 shows $\tau_{\mathrm{MFP}}/\tau_D$ as a function of τ_m/τ_D for fixed values of τ_1/τ_D, τ_2/τ_D. In all three plots, the MFPT displays a similar τ_m/τ_D-dependence as the single-exponential case, c.f. Fig. 4 (a). For $\tau_2/\tau_D = 0.01$ we see in Fig. 10 (a) that $\tau_{\mathrm{MFP}}/\tau_D$ is almost independent of τ_1/τ_D, consistent with the picture that $\tau_{\mathrm{MFP}}/\tau_D$ is determined by the shorter memory time τ_2. On the other hand, for large $\tau_2/\tau_D = 10$ the MFPT shown in Fig. 10 (c) depends very much on τ_1/τ_D and is qualitatively identical to the single-exponential MFPT shown in Fig. 4 (a). Also for this case, we see that the crossover formula Eq. (7) remains accurate.

Appendix G: Comparison of numerical data to Eq. (7) for varying barrier height βU_0

In Fig. 11 we compare predictions of the crossover formula Eq. (7) for τ_{MFP} to numerical results, varying the barrier height βU_0. While Fig. 11 (a) considers the symmetric case ($\tau_\Gamma \equiv \tau_1 = \tau_2$), Fig. 11 (b) considers the asymmetric scenario ($0.001 = \tau_1/\tau_D \ll \tau_2/\tau_D = 10$). The agreement between Eq. (7) and numerical data in Fig. 11 shows that our heuristic formula accurately describes the Langevin data for barrier heights larger than $\beta U_0 \approx 2$ throughout.

[1] H. A. Kramers, Physica **7**, 284 (1940).
[2] D. Chandler, Journal of Statistical Physics **42**, 49 (1986).
[3] B. J. Berne, M. Borkovec, and J. E. Straub, Journal of Physical Chemistry **92**, 3711 (1988).
[4] P. Hnggi, P. Talkner, and M. Borkovec, Reviews of Modern Physics **62**, 251 (1990).
[5] R. Best and G. Hummer, Physical Review Letters **96** (2006), 10.1103/PhysRevLett.96.228104.
[6] R. Zwanzig, Physical Review **124**, 983 (1961).
[7] H. Mori, Progress of Theoretical Physics **33**, 423 (1965).
[8] G. Jung, M. Hanke, and F. Schmid, Journal of Chemical Theory and Computation **13**, 2481 (2017), pMID: 28505440, https://doi.org/10.1021/acs.jctc.7b00274.
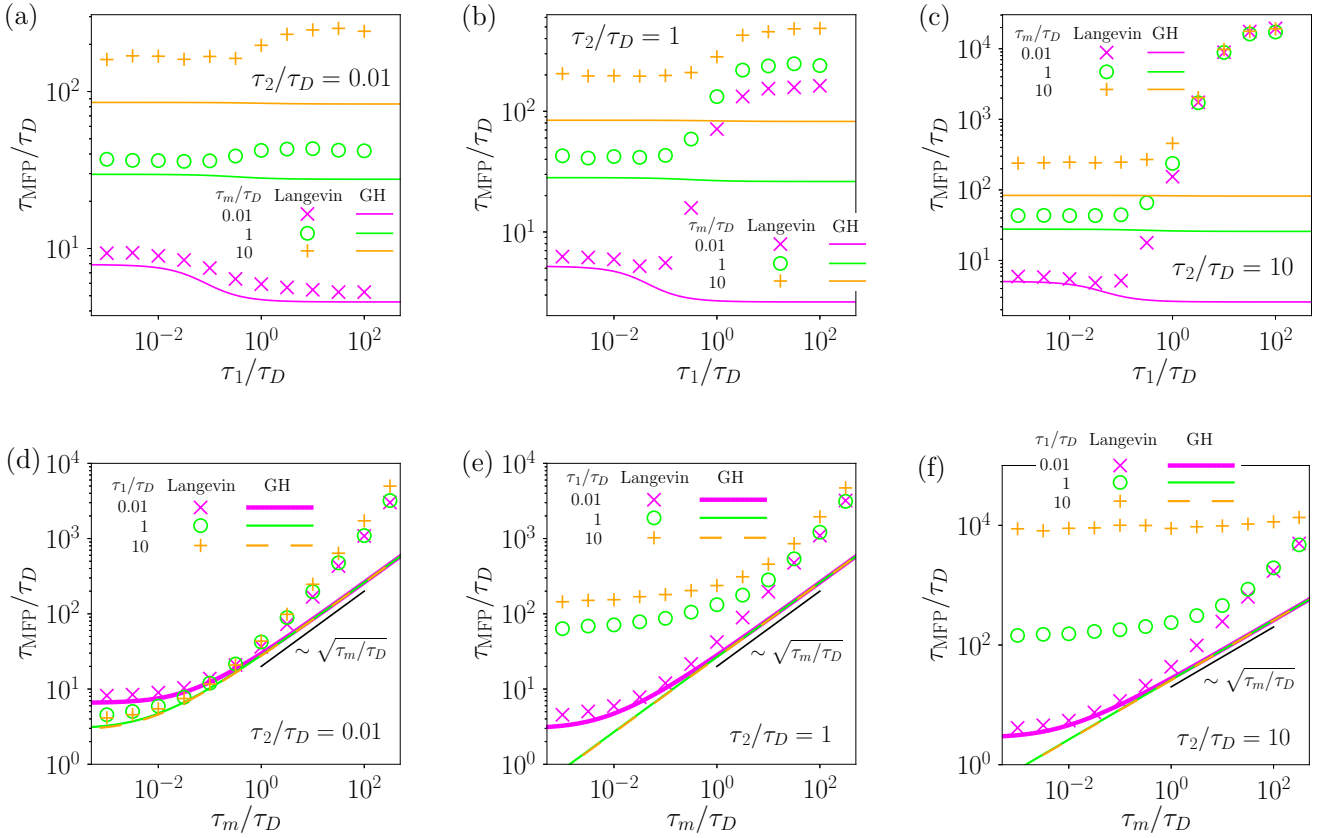
FIG. 7. Comparison of numerical MFPTs to Grote-Hynes (GH) theory. (a)-(c) Colored symbols denote the rescaled MFPT $\tau_{\mathrm{MFP}}/\tau_D$ as function of τ_1/τ_D for several values of τ_2/τ_D and fixed τ_m/τ_D, given by (a) $\tau_m/\tau_D = 0.01$, (b) $\tau_m/\tau_D = 1$, (c) $\tau_m/\tau_D = 10$. The numerical data is the same as shown in Fig. 8. The colored lines represent GH theory, evaluated for a bi-exponential memory kernel using the simulation parameters. (d)-(f) Colored symbols denote the rescaled MFPT $\tau_{\mathrm{MFP}}/\tau_D$ as function of τ_m/τ_D for several values of τ_2/τ_D and fixed τ_1/τ_D, given by (a) $\tau_1/\tau_D = 0.01$, (b) $\tau_1/\tau_D = 1$, (c) $\tau_1/\tau_D = 10$. The numerical data is a replot of the data shown in Fig. 10. The colored lines represent GH theory, evaluated for a bi-exponential memory kernel using the simulation parameters. The black lines indicate the transition-state-theory (TST) scaling $\tau_{\mathrm{MFP}}/\tau_D \sim \sqrt{\tau_m/\tau_D}$ which GH theory attains in the energy-diffusion regime [29]. All data is obtained using $\beta U_0 = 3$.

[9] G. Jung, M. Hanke, and F. Schmid, Soft Matter **14**, 9368 (2018).

[10] H. Meyer, T. Voigtmann, and T. Schilling, The Journal of Chemical Physics **147**, 214110 (2017), https://doi.org/10.1063/1.5006980.

[11] H. Meyer, T. Voigtmann, and T. Schilling, The Journal of Chemical Physics **150**, 174118 (2019), https://doi.org/10.1063/1.5090450.

[12] R. Rey and E. Guardia, The Journal of Physical Chemistry **96**, 4712 (1992).

[13] R. G. Mullen, J.-E. Shea, and B. Peters, Journal of Chemical Theory and Computation **10**, 659 (2014).

[14] R. O. Rosenberg, B. J. Berne, and D. Chandler, Chemical Physics Letters **75**, 162 (1980).

[15] D. de Sancho, A. Sirur, and R. B. Best, Nature Communications **5** (2014), 10.1038/ncomms5307.

[16] J. O. Daldrop, J. Kappler, F. N. Brnig, and R. R. Netz, Proceedings of the National Academy of Sciences **115**, 5169 (2018).

[17] T. G. Mason and D. A. Weitz, Physical Review Letters **74**, 1250 (1995).

[18] D. Lesnicki, R. Vuilleumier, A. Carof, and B. Rotenberg, Physical Review Letters **116** (2016), 10.1103/PhysRevLett.116.147804.

[19] J. O. Daldrop, B. G. Kowalik, and R. R. Netz, Physical Review X **7** (2017), 10.1103/PhysRevX.7.041065.

[20] J. Berner, B. Müller, J. R. Gomez-Solano, M. Krüger, and C. Bechinger, Nature Communications **9**, 999 (2018).

[21] D. Selmeczi, S. Mosler, P. H. Hagedorn, N. B. Larsen, and H. Flyvbjerg, Biophysical Journal **89**, 912 (2005).

[22] G. Wilemski and M. Fixman, The Journal of Chemical Physics **60**, 878 (1974).

[23] A. Szabo, K. Schulten, and Z. Schulten, The Journal of Chemical Physics **72**, 4350 (1980).

[24] A. Dua and R. Adhikari, Journal of Statistical Mechanics: Theory and Experiment **2011**, P04017 (2011).

[25] J. Gowdy, M. Batchelor, I. Neelov, and E. Paci, The Journal of Physical Chemistry B **121**, 9518 (2017).

[26] T. Gurin, O. Bnichou, and R. Voituriez, Nature Chemistry **4**, 568 (2012).

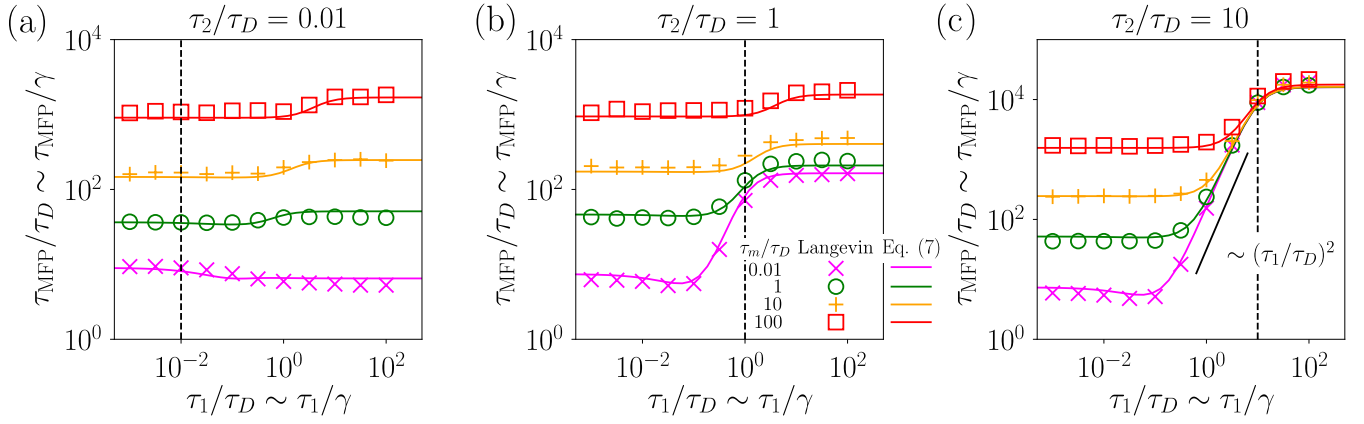[27] S. S. Plotkin and P. G. Wolynes, Physical Review Letters **80**, 5015 (1998).

FIG. 8. Simulation results for the MFPT at fixed τ_2/τ_D. Colored symbols denote the rescaled MFPT $\tau_{\mathrm{MFP}}/\tau_D$ as function of τ_1/τ_D for several values of τ_m/τ_D and fixed τ_2/τ_D, given by (a) $\tau_2/\tau_D = 0.01$, (b) $\tau_2/\tau_D = 1$, (c) $\tau_2/\tau_D = 10$. The legend for all subplots is given in subplot (b). The colored lines represent the crossover formula Eq. (7), the vertical dashed lines denote where $\tau_1 = \tau_2$. The black bar in (c) indicates the scaling $\tau_{\mathrm{MFP}} \sim \tau_1^2$ which corresponds to the single-exponential long-memory regime. All data is obtained using $\beta U_0 = 3$.
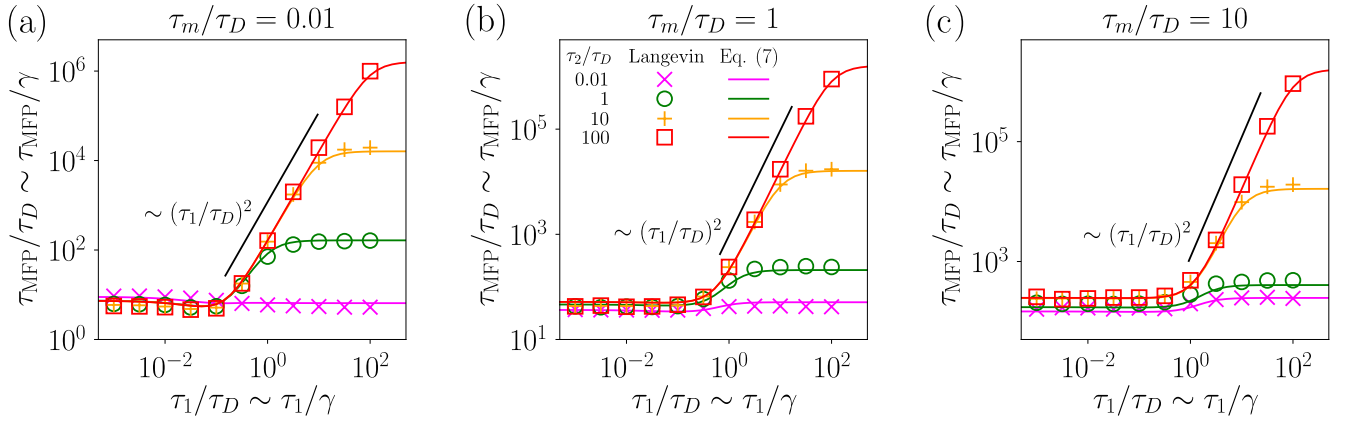

FIG. 9. Simulation results for the MFPT at fixed τ_m/τ_D. Colored symbols denote the rescaled MFPT $\tau_{\mathrm{MFP}}/\tau_D$ as function of τ_1/τ_D for several values of τ_2/τ_D and fixed τ_m/τ_D, given by (a) $\tau_m/\tau_D = 0.01$, (b) $\tau_m/\tau_D = 1$, (c) $\tau_m/\tau_D = 10$. The legend for all subplots is given in subplot (b). The colored lines represent the crossover formula Eq. (7), the black bars indicate the scaling $\tau_{\mathrm{MFP}} \sim \tau_1^2$, which corresponds to the single-exponential long-memory regime. All data is obtained using $\beta U_0 = 3$.

[28] A. Das and D. E. Makarov, J. Phys. Chem. B **122**, 9049 (2018).

[29] R. F. Grote and J. T. Hynes, The Journal of Chemical Physics **73**, 2715 (1980).

[30] B. Carmeli and A. Nitzan, Physical Review Letters **49**, 423 (1982).

[31] J. E. Straub, M. Borkovec, and B. J. Berne, The Journal of Chemical Physics **84**, 1788 (1986).

[32] P. Talkner and H.-B. Braun, The Journal of Chemical Physics **88**, 7537 (1988).

[33] E. Pollak, H. Grabert, and P. Hnggi, The Journal of Chemical Physics **91**, 4073 (1989).

[34] R. Ianconescu and E. Pollak, The Journal of Chemical Physics **143**, 104104 (2015).

[35] S. C. Tucker, M. E. Tuckerman, B. J. Berne, and E. Pollak, The Journal of Chemical Physics **95**, 5809 (1991).

[36] J. Kappler, J. O. Daldrop, F. N. Brnig, M. D. Boehle, and R. R. Netz, The Journal of Chemical Physics **148**, 014903 (2018).

[37] I. S. Tolokh, G. W. N. White, S. Goldman, and C. G. Gray, Molecular Physics **100**, 2351 (2002).

[38] F. Gottwald, S. Karsten, S. D. Ivanov, and O. Khn, The Journal of Chemical Physics **142**, 244110 (2015).

[39] S. H. Northrup and J. T. Hynes, The Journal of Chemical Physics **73**, 2700 (1980).

[40] R. Zwanzig, Journal of Statistical Physics **9**, 215 (1973).

[41] R. Baron, D. Trzesniak, A. H. de Vries, A. Elsener, S. J. Marrink, and W. F. van Gunsteren, ChemPhysChem **8**, 452 (2007).

[42] D. A. Potoyan, A. Savelyev, and G. A. Papoian, WIREs Comput Mol Sci **3**, 69 (2013).

[43] D. Marx, M. E. Tuckerman, J. Hutter, and M. Parrinello, Nature **397**, 601 (1999).

[44] J. O. Daldrop, M. Saita, M. Heyden, V. A. Lorenz-Fonfria, J. Heberle, and R. R. Netz, Nature Communications **9** (2018), 10.1038/s41467-017-02669-9.
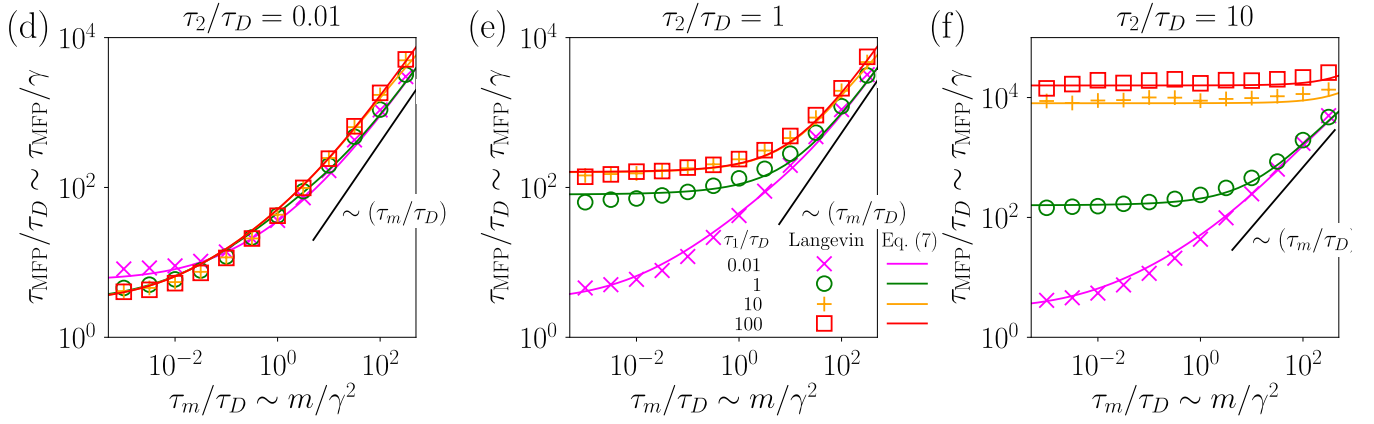
FIG. 10. Simulation results for the MFPT at fixed τ_2/τ_D. Colored symbols denote the rescaled MFPT $\tau_{\mathrm{MFP}}/\tau_D$ as function of τ_m/τ_D for several values of τ_1/τ_D and fixed τ_2/τ_D, given by (a) $\tau_2/\tau_D = 0.01$, (b) $\tau_2/\tau_D = 1$, (c) $\tau_2/\tau_D = 10$. The legend for all subplots is given in subplot (b). The colored lines represent the crossover formula Eq. (7), the black bars indicate the scaling $\tau_{\mathrm{MFP}} \sim \tau_m$ which corresponds to the Markovian inertial regime. All data is obtained using $\beta U_0 = 3$.
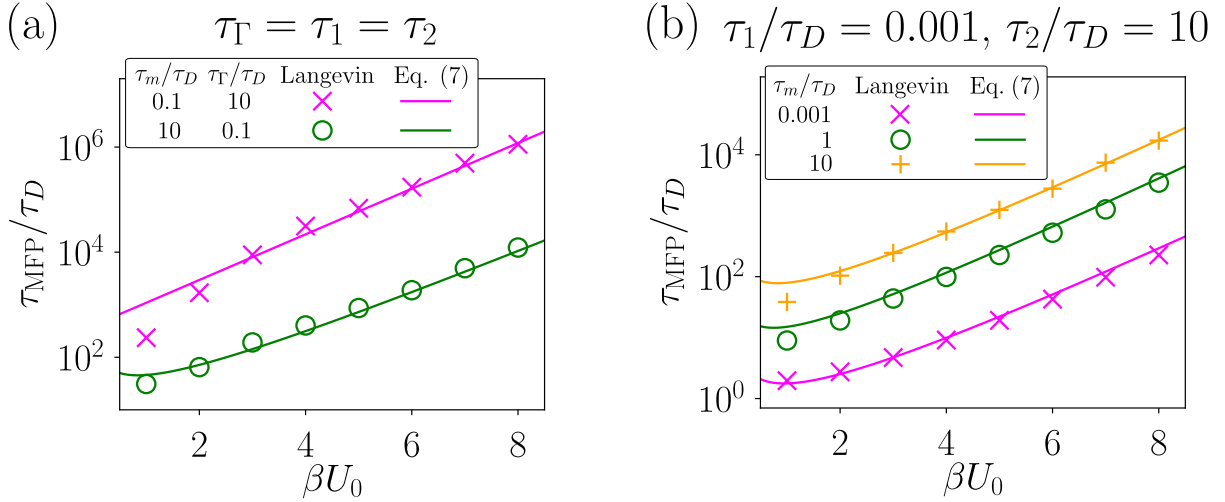

FIG. 11. Simulation results for the MFPT as a function of barrier height βU_0. Colored symbols denote the rescaled MFPT $\tau_{\mathrm{MFP}}/\tau_D$, obtained from numerical simulations, as function of βU_0 for fixed values of τ_m/τ_D, τ_1/τ_D, τ_2/τ_D; colored solid lines represent the crossover formula Eq. (7). (a) Symmetric scenario $\tau_\Gamma \equiv \tau_1 = \tau_2$. (b) Asymmetric scenario with $\tau_1/\tau_D = 0.001$, $\tau_2/\tau_D = 10$. Note that the symmetric scenario has previously been considered in the literature [36].

[45] H. S. Chung and W. A. Eaton, Nature **502**, 685 (2013).
[46] M. Laleman, E. Carlon, and H. Orland, J. Chem. Phys. **147**, 214103 (2017).
[47] V. I. Melnikov and S. V. Meshkov, The Journal of Chemical Physics **85**, 1018 (1986).
[48] P. Hänggi and U. Weiss, Phys. Rev. A **29**, 2265 (1984).
[49] B. Carmeli and A. Nitzan, Phys. Rev. A **29**, 1481 (1984).

[50] J. E. Straub, M. Borkovec, and B. J. Berne, The Journal of Chemical Physics **83**, 3172 (1985), https://doi.org/10.1063/1.449172.
[51] H. Grabert, P. Schramm, and G.-L. Ingold, Physics Reports **168**, 115 (1988).
[52] J. Kappler, F. Noé, and R. R. Netz, Phys. Rev. Lett. **122**, 067801 (2019).
[53] D. Marx, ChemPhysChem **7**, 1848 (2006).
[54] P. Reimann, G. J. Schmid, and P. Hnggi, Physical Review E **60**, R1 (1999).